MORPHOLOGY ANALYSIS OF LEAD IODIDE- AND LEAD ACETATE-BASED PEROVSKITE LAYERS FOR SOLAR CELL APPLICATION

A Thesis Submitted to the Department of Materials Science and Engineering

African University of Science and Technology

In Partial Fulfilment of the Requirements for the Degree of MASTER of Science

By

Osawemwenze Amen Lilian

Abuja, Nigeria

2018

CERTIFICATION

This is to certify that the thesis titled “Morphology Analysis of Lead Iodide- and Lead Acetate-Based Perovskite Layers for Solar Cell Application” submitted to the school of postgraduate studies, African University of Science and Technology (AUST), Abuja, Nigeria for the award of the Master's degree is a record of original research carried out by Lilian Amen Osawemwenze in the Department of Materials Science and Engineering.

MORPHOLOGY ANALYSIS OF LEAD IODIDE- AND LEAD ACETATE-BASED PEROVSKITE LAYERS FOR SOLAR CELL APPLICATION

By

Osawemwenze Amen Lilian

A THESIS APPROVED BY THE DEPARTMENT OF MATERIALS SCIENCE AND ENGINEERING

RECOMMENDED: _____

Supervisor, Prof. Esidor Ntsoenzok

_____

Cosupervisor, Dr. M.G. Zebaze Kana

_____

Member, Dr. Vitalis Anye

_____

Head, Department of material Science and Technology

APPROVED: _____

Chief Academic Officer

_____

December 9th, 2017

ABSTRACT

Organolead trihalide perovskite solar cells have shown success as light absorbers in photovoltaic cells due to their efficiency increasing from 3.5% to over 20% within only five years. However, pinhole formation and incomplete coverage of solution-processed perovskite film results in increased current leakage, reducing efficiency. Hence the surface morphology of perovskite film is important for high performance of perovskite solar cells. Here the morphology is carefully controlled by varying processing conditions, perovskite films were prepared using two different lead sources: lead acetate ($Pb(OAc)_2$) and lead iodide (PbI_2), with methylammonium iodide (CH_3NH_3I) as the source material. The structural, optical and absorbance properties of the perovskite films varied with the lead sources used, perovskite from a $Pb(OAc)_2.3H_2O$ source annealed at 90^oC gave the best structure compared to $Pb(OAc)_2.3H_2O$ annealed at 80^oC and anhydrous $Pb(OAc)_2$ annealed at 90^oC. The perovskite film from the PbI_2 source did not have smooth film, pinholes were formed with low crystallinity, a small amount of $Pb(OAc)_2$ (about 5% mol) was added to the PbI_2 in the solution, this improved the film crystallinity. The perovskite film derived from lead acetate showed enhanced surface coverage with quality crystalline film.

Keywords: Solar cell, perovskite, lead acetate, lead iodide, pinholes, structure, morphology.

ACKNOWLEDGEMENT

I give all thanks and praise to God Almighty for blessing me with life, health, wisdom, strength and divine favour, to enable me carry out my master's program and thesis successfully. I am who I am today by His Grace, Love and Mercies.

My heartfelt gratitude goes to my supervisor Prof. Esidor Ntsoenzok for his devoted guidance, time, patience, encouragement and support, which led to the success of this research. He believed in me and my ability to carry out any responsibility, and continues to show interest in my career. His interest and enthusiasm for science and renewable energy was a source of inspiration.

I also wish to express my appreciation to Dr. Zebaze Kana for his contributions during my preparation for this research work. Special thanks to Dr. Vitalis Anye for his guidance, support, encouragement and time as the second reader of this thesis. I also thank Dr. Adulhakeem Bello and Dr. Dahiru Sani for their time, support and valuable contributions to this research work which steered me in the right direction. My sample characterisation and analysis were successful because of their valuable input. My gratitude also goes to my mentor Dr. Gideon Adogbo for his insightful comments, encouragement and also for the questions which made me focus my research and view it from various perspectives.

I also wish to thank Prof. Azikiwe Onwualu the head of my department, all my friends, well-wishers and colleagues in the class, especially my research colleague in the energy group Ridwan Ahmed, for their support. Special thanks to Francis Jimoh, Clare Nwazojie and Chinenye Chinwego for their great support. Thanks to all the laboratory technologists in the African University of Science and Technology (AUST) for their technical support. I sincerely thank the Pan African Materials Institute (PAMI) for the grant given to support this research work. I also thank my sponsors AUST, African Capacity Building Fund (ACBF) and the Nelson Mandela Institution (NMI).

Finally, my profound gratitude goes to my families: the Adogbos, the Egbunus, my loving and devoted parents and siblings for their unflinching support, their love, financial support, encouragement and prayers which propelled me through school. I also thank Rev. Kujiyat, his wife and Rhema family. To my Love, David Ajogwu thank you for your love, time, encouragement and patience throughout my study, God bless you all.

Contents

LIST OF TABLES

LIST OF FIGURES

LIST OF ABBREVIATIONS AND SYMBOLS

AM	Air Mass
a-Si	Amorphous silicon
BIPV	Building Integrated Photovoltaics
$CaTiO_3$	Calcium Titanate
CB	Chlorobenzene
CdTe	Cadmium telluride
$CH_3NH_3PbI_3$	Methyl Ammonium Lead tri-iodide
CdIS	Cadmium Indium Selenide
Cs	Caesium
C_{60}	Fullerene
DMF	N,N – Dimethylformamide
DSSCs	Dye-sensitized solar cells
DSVD	Dual-source vacuum thermal evaporation
ETL	Electron Transfer Layer
F8TB	Poly(9,9'-dioctylfluorene-co-bis-N,N'-(4-butylphenyl)-bis-N,N'-phenyl-1,4- phenylenediamine
$FAPbI_3$	Formamidinium lead iodide
FDC	Fast deposition crystallization
FF	Fill factor
F_dTO	Fluorine-doped titanium oxide
GaAs	Gallium Arsenide
GBL	Gamma butyrolactone
HI	Hydriodic
HOMO	Highest occupied molecular orbital
HTL	Hole Transfer Layer
I_m	Maximum Current
I_{sc}	Short circuit current
ICBA	Indene-C60 Bisadduct

InP	Indium Phosphide
IPA	Isopropyl alcohol
IR	Infra-red
ITO	Indium Tin Oxide
I_dTO	Indium-doped titanium oxide
J_{sc}	Short-circuit current density
Li-TFSI	Bis(trifluoromethane) sulfonimide lithium salt
LUMO	Lowest unoccupied molecular orbital
MAAc	Methyl ammonium acetate
MACl	Methyl ammonium chloride
MAI	Methyl Ammonium Iodide
mc-silicon	Multi-crystalline silicon
MEG	Multiple Exciton Generation
MEH-PPV	Poly[2-methoxy-5-(2'-ethyl-hexyloxy)-1,4-phenylene vinylene]
NREL	National Renewable Energy Laboratory
OECD	Organization for Economic Cooperation and Development
P3HT	Poly(3-hexylthiophene)
P3OT	Poly(3-octylthiophene)
$Pb(Ac)_2$	Lead acetate
PbI_2	Lead Iodide
$(Pb(OAc)_2•3H_2O$	Lead acetate trihydrate
$PbCl_2$	Lead chloride
PC60BM	6,6-phenyl-C61-butric acid methyl ester
PC70BM	6,6-phenyl-C71-butric acid methyl ester
PCE	Power Conversion Efficiency
PFO	Polyfluorene
PFODBT	Poly[2,7-(9,9-dioctyl-fluorene)-alt-5,5-(4,7'-di-2-thienyl-2',1',3',-benzothiadiazole)
PSC	Perovskite Solar Cell
PPV	Polyphenylenevinylene
PTAA	Poly[bis(4-phenyl)(2,4,6-trimethylphenyl)

PV	Photovoltaic
Spiro-OMeTAD	2,2′,7,7′-tetrakis (N,N-di-4-methoxyphenylamino)-9,9′-spirobifluorene
TCO	Transparent conductive oxides
TiO_2	Tin Oxide
TBP	4-tert-butylpyridine
TSC	Tandem Solar Cell
UV	Ultra Violet
V_{oc}	Open-circuit voltage
V_m	Maximum output voltage
VASP	Vapor- assisted solution process
QD	Quantum Dot

CHAPTER ONE: INTRODUCTION

1.1 Background

The growing global population and industrialisation have led to the continuous increase in demand for energy. Global energy demand is predicted to be as high as 1GW/day, which places substantial pressure on current energy infrastructures (Wang, Wright, Elumalai & Uddin, 2016). The supply of fossil fuels is consistently declining and cannot satisfy the huge energy demands in the nearest future. These challenges, in addition to the danger of climate change, have necessitated the development of energy from renewable energy sources, which are environmentally friendly and sustainable. Among the probable renewable energy technologies, photovoltaic (PV) solar cells, which convert sunlight into electricity, provide a promising solution; solar power is the most abundant energy source in the world (Zulkifli & Bahtiar, 2016). A year's worth of sunlight contains 1.5×10^{18} kWh of energy; the known reserves of oil, coal and gas are 1.75×10^{15} kWh, 1.4×10^{15} kWh, and 5.5×10^{15} kWh, respectively (Sum & Mathews, 2014). A year's worth of sunlight provides more energy than the entire known fossil fuel reserve. The challenge is to convert solar energy efficiently and cost-effectively.

Photovoltaic is currently dominated by crystalline silicon solar cells, which are the most efficient solar cells available for commercial use (Bailie et al., 2015). However, they are not cost- effective as the cost of fabrication involves pure and expensive materials, high-technology processing techniques and high temperature processing. This makes crystalline silicon solar cells not economically viable for many applications (Jeon et al., 2014). In order to reduce the processing cost, an alternative approach is to manufacture solar modules using solution processing techniques which significantly reduce costs and the energy payback time (Chen, 2015).

The third-generation technologies, which includes quantum dot (QD) solar cells, polymer solar cells, organic solar cells and dye-sensitised solar cells, involve the fabrication of solar cells through solution processing and low temperature processes; this reduces the production cost (Yang, Barrows, Lidzey & Wang, 2016).

However, their limited absorption and low carrier mobility, limits their achieving commercially viable device efficiencies.

Recently, a new class of materials, organic-inorganic metal halide perovskite solar cells have been discovered, which may be able to address the challenges of low cost without compromising efficiency (Kojima et al., 2009). The perovskite structure has recently been successfully applied in photovoltaics; the efficiency increased from 3.8% in 2009 to 22.1% in 2017 (Woon Seok Yang et al., 2017). The most commonly used organic-inorganic metal halide perovskite is the methylammonium lead triiodide ($CH_3NH_3PbI_3$). The photovoltaic properties of these solar cells are dependent on the crystal structure of the perovskite compound, the fabrication process, the hole transport layer (HTL), the electron transport layer (ETL), the nanoporous layer and interfacial microstructures (Oku, Matsumoto, Suzuki & Suzuki, 2015).

Although perovskite solar cells with the highest power conversion efficiency (PCE) of 22.1% have been reported, it is still a challenge to form a homogeneous pinhole-free perovskite film, which is essential to get reproducible high-efficiency perovskite solar cells (Bella et al., 2016). Material crystallinity and aggregation distribution plays an important role in determining the electronic properties and the performance of both organic and inorganic electronic devices (Bae, Park, Han, Shin & Jo, 2017). This research work is based on morphology optimisation and analysis of the perovskite layer for solar cells, to provide an important pathway for the design of mechanically robust and efficient perovskite solar cells.

1.2 Problem Statement

Solution-processed perovskite film tends to have voids and pinholes between the crystals, which is harmful to device performance. The voids and pinholes cause electrical shorting, negatively impacting charge dissociation/transport/recombination because of the defects on the surface and grain boundaries of the perovskite films, which lead to lost light absorption in the solar cell.

Therefore, the perovskite film must have high quality crystal and large grain size to obtain high carrier lifetime and high charge carrier mobility in order to influence the PCE of the solar cell.

1.3 Aim and Objectives

The aim of this research was to study and optimise the morphology of lead-based perovskite solar cells in order to obtain high coverage and uniform crystalline domain of the perovskite layer resulting in higher PCE.

The objectives were to:

i. Fabricate a thin film CH_3NH_3I/PbI_2 using different lead sources by spin coating on a soda lime glass substrate in a nitrogen-controlled environment and comparing their morphology.
ii. Analyse the change in the optical properties and morphology of the perovskite, based on the lead source used and thermal annealing step.
iii. Determine the phases present, using X-ray diffraction (XRD), and the absorbance, using ultraviolet spectrometry.

1.4 Outline of Thesis

Chapter One provides a general introduction to the current energy needs, solar power and its technologies, and perovskite solar cells. It also includes the aim and objectives of this research work.

Chapter Two is a literature review on the world's energy needs, the energy challenges facing Africa and how the economy is being affected. It also gives a review of the fundamentals and evolution of photovoltaic and solar cells.

Chapter Three presents a detailed review on perovskite solar cells and works by researchers in the field.

Chapter Four describes the experimental procedure carried out. The results obtained, and the discussion of the results, are presented in Chapter Five. The conclusion and recommendations for future work are presented in Chapter Six.

CHAPTER TWO: LITERATURE REVIEW

2.1 Global and African Energy Needs

Energy is an essential constituent for the development of any economy and it is the source of many of the major impacts of human beings on their immediate environment. People consume food, water, minerals, health care and other services as they go about their daily activities, all of which require energy consumption (Holdren, 1991). The Population Division of the United Nations predicts a global population of approximately 9.7 billion people by 2050 (Zabel, 2009). That is over 2 billion more people than the approximately 7.5 billion people the United Nations estimated were alive in August 2017 (Worldometers, 2017). The increase in population will lead to medical advances, improvements in public health, sanitation and hygiene, increased food availability and agricultural productivity, the extension of cultivation and the development of trade and transportation; which indicates that energy demand will increase.

The International Energy Agency (IEA) and the Energy Information Administration (EIA), extrapolating from past and current trends in energy consumption, forecast that the total world energy consumption would rise from 549 quadrillion BTUs in 2012 to 815 quadrillion BTUs in 2040, an increase of 48% (International Energy Agency, 2016). Much of the increase in world energy demand occurs among the developing non-OECD (Organisation for Economic Cooperation and Development) nations, which includes Africa. Population growth determines our energy consumption forecasts. It is predicted that non-OECD demand for energy will rise by 71% from 2012 to 2040, compared to an increase of 18% in OECD nations, refer to Figure 2.1.

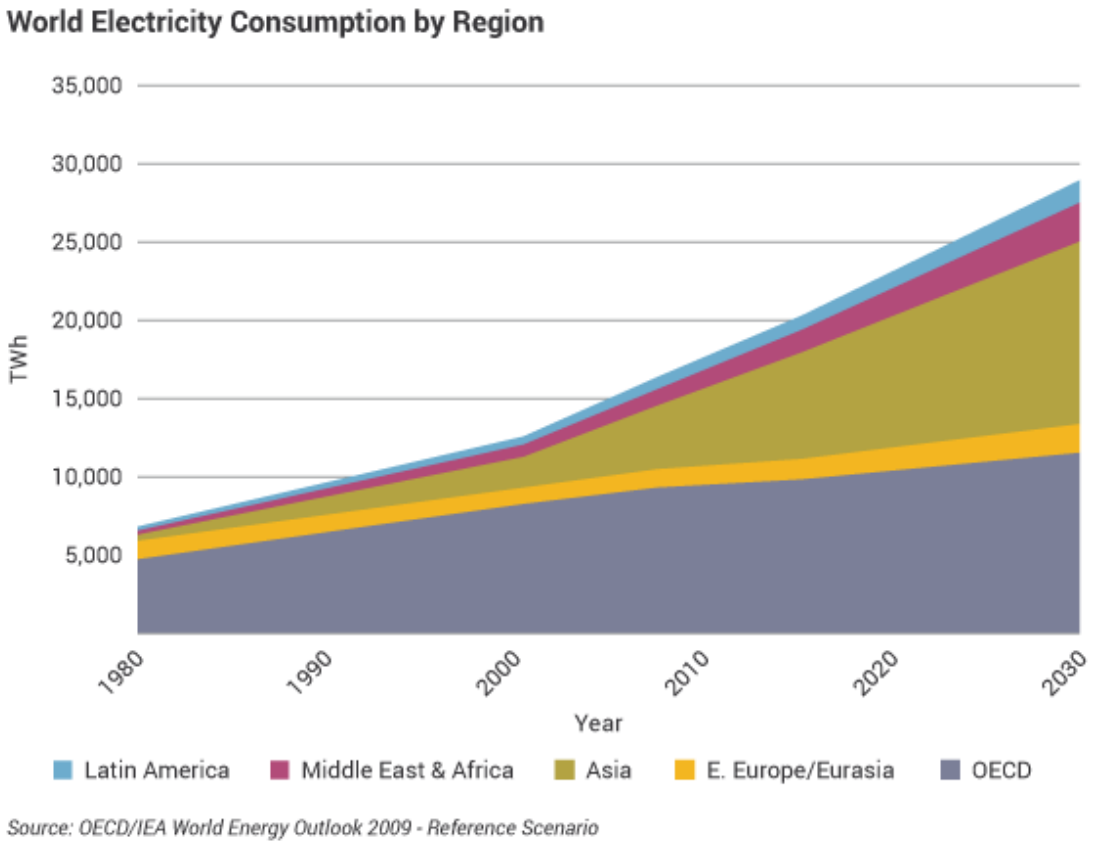

Figure 2.1: World Electricity Consumption by Region (World-nuclear association, 2017)

More than 620 million people in sub-Saharan Africa (two-thirds of the population) live without electricity. Africa has not been able to meet the present energy need, resulting in an under-developed economy. Africa has the most potential for solar power, roughly 40% of Africa's surface receives over 2000 kilowatts per hour of solar energy annually (Liu, 2015). It is, therefore, imperative for Africa to take advantage of the rich solar energy supply to meet the growing population and energy demand for improved economic development (Jimoh, 2014). Globally, the sun's energy supply needs to be harnessed in an efficient and cost-effective way to meet the projected increase in global energy demand.

2.2 Solar Energy

Solar energy is radiant light and heat from the sun that can be harnessed using various technologies for applications such as heating of water, solar thermal power stations and photovoltaic panels. It is a renewable energy source. The sun emits a great amount of energy in the form of electromagnetic radiation into space (NREL, 2017).

The sun emits 3.8×10^{26} watts (W) of electromagnetic power from gamma rays to radio wavelengths, with most of the energy emitted in the visible light spectrum between 400 nanometers and 700 nanometers (Odenwald, 2017). The amount of energy emitted each second equals 3.8×10^{26} joules (J). The intensity of solar radiation is about 6.33×10^{7} W/m^2. On average, each square metre of land is exposed to enough sunlight to produce 1,700 kWh of power every year (ITACA, 2017). As the sun's rays spread out into space, the radiation becomes less intense, only a fraction of the emitted energy reaches the earth's surface. The losses are due to absorption by the earth's atmosphere, in other words, the ozone, water vapour, nitrogen, oxygen and carbon dioxide prevent the ultraviolet (UV) and some parts of the infrared (IR) portion of the solar spectrum from reaching the earth's surface.

The air mass is an extremely large body of air whose properties of temperature and moisture content (humidity), at any given altitude, are mostly uniform in any horizontal direction (National Geographic Society, 2017). The air mass coefficient (AM1.5) is an index used to determine the effective electromagnetic radiation emitted by the sun at sea level. It denotes the maximum amount of energy that is available for a solar cell to convert into electrical current. The maximum irradiance peak in the AM1.5 spectrum is in the visible light region, nonetheless an ideal solar cell should be able to convert the whole of the spectrum in order to maximise the yield of the current generated (Bastiani, 2016), refer to Figure 2.2.

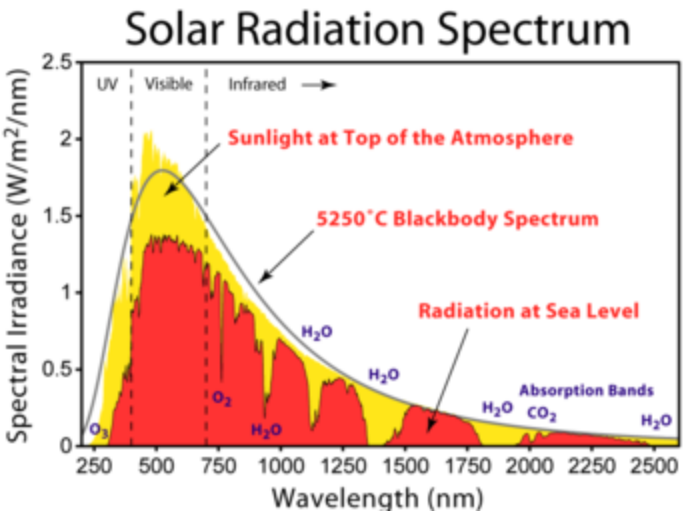

Figure 2.2: Solar irradiance spectrum above the atmosphere and at the surface (Majka & Majka, 2013)

2.3 Photovoltaics

Photovoltaics (PV) is the direct conversion of light into electricity at the atomic level. Some materials exhibit a property known as the photoelectric effect that causes them to absorb photons of light and release electrons. When these free electrons are captured, an electric current results that can be used as electricity (Green Energy, 2015).

When semiconductor materials are exposed to light, some of the photons of light rays are absorbed by the semiconductor crystal, which causes a significant number of free electrons and holes in the crystal. The free electrons and holes can recombine if there is no driving force; hence the solar cell must provide an internal electric field to transport the electrons and holes in opposite directions. The two fundamental processes of PV effect namely, light absorption and charge separation, are the basis of all inorganic PV cells; this is the basic principle of producing electricity due to photovoltaic effect (Vatansever, Siores & Shah, 2012). Electric current generation takes place in the depletion zone or PN junction, where electrons from the N-type silicon occupy the holes of the P-type electron. When a photon of light ray is absorbed by one of the atoms of the N-type silicon, an electron is displaced creating a free electron and a hole. The free electrons are attracted to the free holes when a metal wire is connected to the cathode (N-type silicon) and the anode (P-type silicon).

The electrons flow from the N-type layer to the P-type layer by crossing the depletion zone and then through the external wire back of the N-type layer, creating a flow of electricity (American Chemical Society, 2014), refer to Figure 2.3.

Solar cells have evolved over the years in a bid to convert the sun's energy to power efficiently with the least cost. Solar cells can therefore be divided into three generations, namely: first, second and third generations.

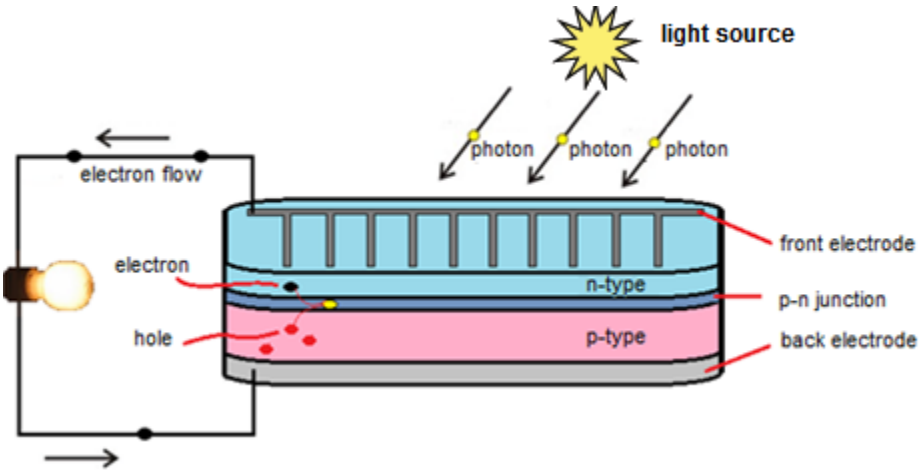

Figure 2.3: Layers and working principle of a silicon solar cell (Vatansever et al., 2012)

2.4 Electrical Characteristics of Photovoltaic

Three important parameters that characterise the performance of a photovoltaic cell are the short-circuit current (I_{sc}), the open-circuit voltage (V_{OC}), and the fill factor (FF) (Jasim, 2015).

2.4.1 Short Circuit Current

This is the current through the solar cell, when the voltage across the solar cell is zero. The short circuit current (I_{sc}) is due to the generation and collection of light-generated carriers (Baghzouz, 2017). The I_{sc} depends on the area of the solar cell, the power of the incident light, the spectrum of the incident light, the optical properties of the solar cell and the collection probability of the solar cell.

Short-circuit current density (J_{sc}) is used in the stead of short circuit current to remove the dependency of the solar cell area on I_{sc}. The maximum current that the solar cell can supply strongly depends on the optical properties of the solar cell, such as absorption in the absorber layer and reflection (Chritiana Honsberg & Stuart Bowden, 2017a). The collection probability depends mainly on surface passivation of the solar cell to prevent surface recombination of a photo-excited electron hole pair (Bonilla, Reichel, Hermle, Senkader & Wilshaw, 2012). The short circuit current is the largest current which can be drawn from the solar cell (Alternative Energy, 2017).

The short circuit current density (J_{SC}) depends on the generation rate and the diffusion length of electrons and holes, which is shown in Equation 1:

$$J_{SC} = qG(L_n + L_p) \qquad \text{Equation 1}$$

Where G is the generation rate, q is the absolute value of the electron charge, and Ln and Lp are the electron and hole diffusion lengths respectively (Chritiana Honsberg & Stuart Bowden, 2017a).

2.4.2 Open-circuit Voltage

The open-circuit voltage (V_{OC}) is the maximum voltage available from a solar cell, when it is not connected to any load (zero current) (Alternative Energy, 2017). The total rate of photo-generation in the solar cell is equal to the rate of recombination so that no current circulates through the circuit. The open-circuit voltage corresponds to the amount of forward bias on the solar cell due to the bias of the solar cell junction with the light-generated current. Equation 2 for V_{OC} is obtained by equating the net current to zero in the solar cell equation to give:

$$V_{OC} = \frac{nkT}{q} In(\frac{I_L}{I_O} + 1) \qquad \text{Equation 2}$$

Where K is the Boltzmann's constant, T is the absolute temperature, n is the ideality factor, q is the absolute value of the electron charge, I_L is the photo-generated current and I_O is the reverse saturation current or dark saturation current.

2.4.3 Fill Factor (FF)

The FF is a measure of quality of a solar cell, it determines the maximum power from a solar cell when combined with V_{OC} and I_{SC} (Christiana Honsberg & Stuart Bowden, 2017b). The FF is defined as the ratio of the maximum power (I_{mp} x V_{mp}) from the solar cell to the product of V_{OC} and I_{SC} (the theoretical power) (Alternative Energy, 2017). When analysed graphically, see Figure 2.4, the FF is a measure of the "squareness" of the I-V curve. It can be calculated from Equation 3:

$$FF = \frac{V_m I_m}{I_{sc} V_{oc}} \qquad \text{Equation 3}$$

Where V_m and I_m are the maximum output voltage and current, respectively.

A solar cell with a higher voltage has a larger possible FF, the closer the FF is to unity, the more power the PV can provide. FFs range from 0.5 to 0.82 (National Instruments, 2017).

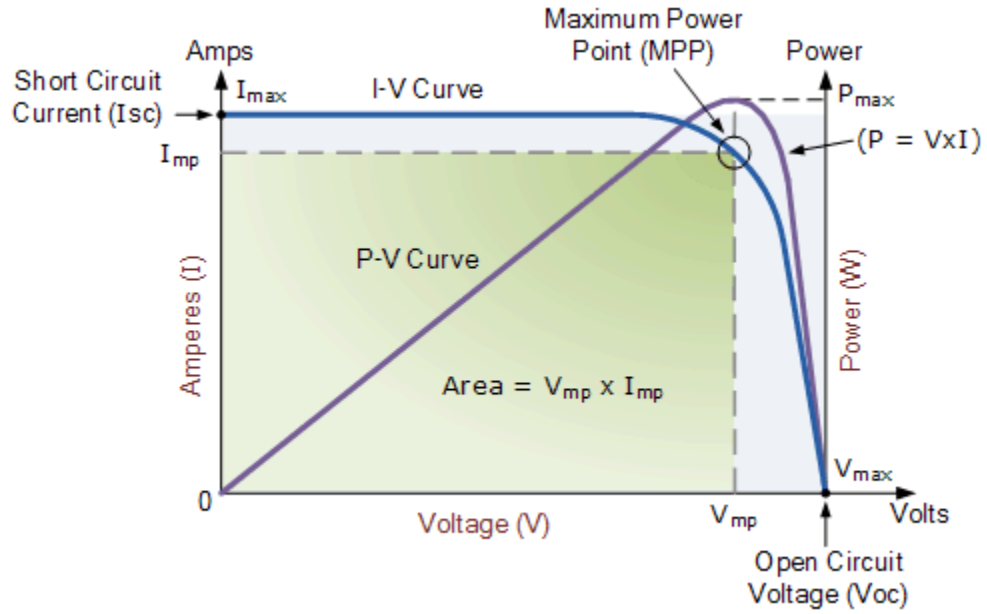

Figure 2.4: Solar Cell I-V characteristic curve (Alternative Energy, 2017)

2.4.4 Power Conversion Efficiency (PCE)

The PCE of a solar cell is the ratio of energy output (P_{out}) from the solar cell to the sun input energy (P_{in}) (Honsberg, & Bowden, 2017c). The solar cell can be operated up to its maximum power output to get the maximum efficiency, therefore, P_{out} can be taken to be $P_{max.}$ The sun input energy (P_{in}) is the product of the irradiance of the incident light, measured in W/m^2 or in suns (1000 W/m^2), with the surface area of the solar cell (m^2). The maximum efficiency (η_{max}) of a solar cell can also be affected by temperature and the intensity and spectrum of the incident light (National Instruments, 2017). The efficiency of a solar cell can be calculated from Equation 4:

$$\eta = \frac{P_{\max}}{P_{in}} = \frac{V_{oc} I_{sc} FF}{P_{in}} \qquad \text{Equation 4}$$

2.5 Evolution of Solar Cells

2.5.1 First-Generation Solar Cells

The first generation of solar cells were the silicon wafers; the advantage of silicon is its mature fabrication technology, its large abundance in the earth and its non-toxicity. The band gap of silicon is 1.11 eV, which is close to the optimal bandgap of 1.3 eV for maximum photo conversion efficiency of 33% in a single-junction solar cell, as determined by Shockley and Queisser (Wadia, Alivisatos & Kammen, 2009). The silicon solar cell can be single-crystal or multi-crystal, the silicon wafer has only one grain in a single or mono-crystal solar cell, while multi-crystal solar cells have wafers with many grains with distinct grain boundaries. The highest performance for single crystals is 25% as certified by the National Renewable Energy Laboratory (NREL) (Jacoby, 2016) and each wafer can supply 2–3 watt power (Kibria, Ahammed, Sony, Hossain & Shams-Ul-Islam, 2015). Conventional silicon cells require ultra-high-purity silicon in the order of 99.999% purity, which is the single crystalline silicon. These cells are made through energy-intensive crystal growth and vapour deposition methods, which adds to their costs (Badawy, 2015).

High costs and the sophisticated technological steps have led to the use of polycrystalline silicon (multi-crystal) instead of the single-crystal wafers, but at the

expense of solar conversion efficiency. Multi-crystalline silicon (mc-silicon) has a wider use than single-crystal silicon because of the cost reduction, the conversion efficiencies of commercial silicon were in the range of 15–17%, although a higher efficiency of 20.4% was certified by NREL in 2004 (Chen, 2015). The improvement of the efficiency increased the commercial viability of multi-crystalline silicon and currently silicon has about 90% of the solar market. Continuous research in the bid to reduce cost without compromising efficiency led to the development of the second-generation solar cells.

2.5.2 Second-Generation Solar Cell

The second-generation solar cells centred on thin film technology with different materials being used (Badawy, 2015). The materials used as light absorbers are composed of thin layers; the film thickness differs from a few nanometers (nm) to tens of micrometres (μm), and includes amorphous silicon (a-Si), cadmium indium selenide (CdIS), cadmium telluride (CdTe), copper indium gallium selenide (CIGS), gallium arsenide (GaAs) and thin silicon films on indium tin oxide. They have energy bandgaps within the range of 1.1 – 1.7 eV (Vatansever et al., 2012). The thin layer solar cells give the advantage of cost reduction in the manufacturing process due to lower material consumption and low temperature processing compared to the conventional silicon. The highest lab efficiency in thin film technology is 21.7% for CIGS and 21.0% for CdTe solar cells. In the last decade, the efficiency of commercial CdTe increased from 9% to 16% (ISE, 2017). Thin-film solar cells can be grown on a flexible substrate, which is used for building-integrated photovoltaics (BIPV), such as windows of houses and cars (Meillaud et al., 2015). The limitation of this technology is that some of the solar cells are based on scarce elements, which makes price a limiting factor; have lower efficiency rates and there is less experience of the modules' lifetime performance (EPIA & GreenPeace, 2006). The market share of all thin film solar cells was about 6% of the total annual production in 2016 (ISE, 2017).

2.5.3 Third-Generation Solar Cell

Research is ongoing to find a high performance photovoltaic with a lower cost per watt of electricity generated; the cost of the inorganic materials and the fabrication

technology is too high for quick commercial scale up. The third-generation solar cells do not have a P-N junction, they work based on donor-acceptor interfaces (Fru, 2016) and are solution processable solar cells. They include organic solar cells, nanocrystal-based solar cells, polymer-based solar cells, dye-sensitised solar cells, concentrated solar cells and tandem/multi-junction cells (Yan & Saunders, 2014). These novel technologies have the potential to contribute to sustainable energy systems but are not commercially proven yet. The production cost and raw materials of these solar cells and their efficiencies are low.

2.5.3.1 Organic Solar Cells

This PV cell technology uses organic, electronic conductive polymers or small molecules for light absorption and electrical charge transport (Bagher, 2014). The semiconducting polymers used have suitable bandgaps, absorption characteristics and physical properties, they are carbon-based materials comprising alternating C-C and C=C bonds as their backbones (Chen, 2015). The photovoltaic effect of organic PV cells is based on electron transfer from donor-type semiconducting conjugated polymers to acceptor-type conjugated polymers or acceptor molecules. The light absorbing layer, which comprises the electron donor (D) and electron acceptor (A), is sandwiched between transparent anodes with a high work function. For example indium tin oxide (ITO) and a metallic cathode with a low work function which can be magnesium or aluminium (Fru, 2016). The absorption of photons by the donor-type semiconducting polymer leads to the generation of Frankel excitons which diffuse to the donor-acceptor interface. At the interface, the strength of the effective electric field breaks up the excitons into free electrons and free holes by causing the electrons to fall from the lowest unoccupied molecular orbital (LUMO) of the absorber material to the LUMO of the acceptor material with higher electron affinity. The holes are transported to the anode and the electrons to the cathode, thus generating electricity (Bastiani, 2016).

Semiconducting polymers have a lower dielectric constant; hence, the diffusion length of excitons is shorter than that of inorganic PV materials. However, they have a higher extinction constant than inorganic PV.

A thickness of 300 nm is needed by organic materials to absorb the most incident light; however, a minimum thickness of 100 nm is required to maximise light absorption (Vatansever et al., 2012). Electron acceptors with high electron mobility are the most suitable materials for polymer solar cells. Electron acceptor polymers suitable for organic photovoltaics include; 6,6-phenyl-C61-butric acid methyl ester ($PC_{60}BM$), 6,6-phenyl-C71-butric acid methyl ester ($PC_{70}BM$) and poly(9,9'-dioctylfluorene-co-bis-N,N'-(4-butylphenyl)-bis-N,N'-phenyl-1,4-phenylenediamine, (F8TB) (Singh et al., 2005). Suitable electron donor polymers for organic photovoltaics include; poly(3-hexylthiophene) (P3HT), poly(3-octylthiophene) (P3OT), polyphenylenevinylene (PPV), polyfluorene (PFO), poly[2,7-(9,9-dioctyl-fluorene)-alt-5,5-(4,7'-di-2-thienyl-2',1',3',-benzothiadiazole)], (PFODBT), poly[2-methoxy-5-(2'-ethyl-hexyloxy)-1,4-phenylene vinylene], (MEH-PPV) (Yan & Saunders, 2014).

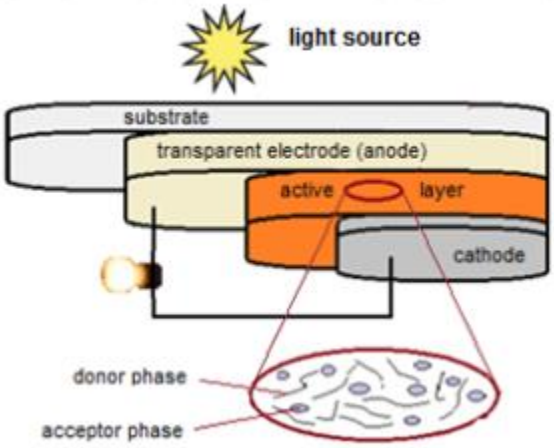

Figure 2.5: Donor-acceptor heterojunction configurations in a typical organic solar cell (Vatansever et al., 2012)

2.5.3.2 Dye-sensitized Solar Cells

Dye-sensitized solar cells (DSSCs) are hybrid solar cells containing a meso-structured inorganic N-type oxide (such as TiO_2) that is sensitised with an organic or metal complex dye, and infiltrated with an organic P-type hole-conductor (M. Liu, Johnston, & Snaith, 2013a).

DSSCs separate the function of charge carrier transport from light absorption, where the dye sensitiser absorbs the incident sunlight ray and uses the light energy to prompt electron transfer reaction (Wei, 2010), refer to Figure 2.6. The electron is injected into the inorganic oxide (TiO_2) where it is transmitted through the TiO_2 nanoparticles to reach an electrode. DSSCs are economical, easy to manufacture and the materials that are used for their fabrication are readily available (Will Soutter, 2013). The highest efficiency record has increased from 7 % in 1991 to about 14 % in 2015 (Lee, Li & Kuo-ChuanHo, 2017).

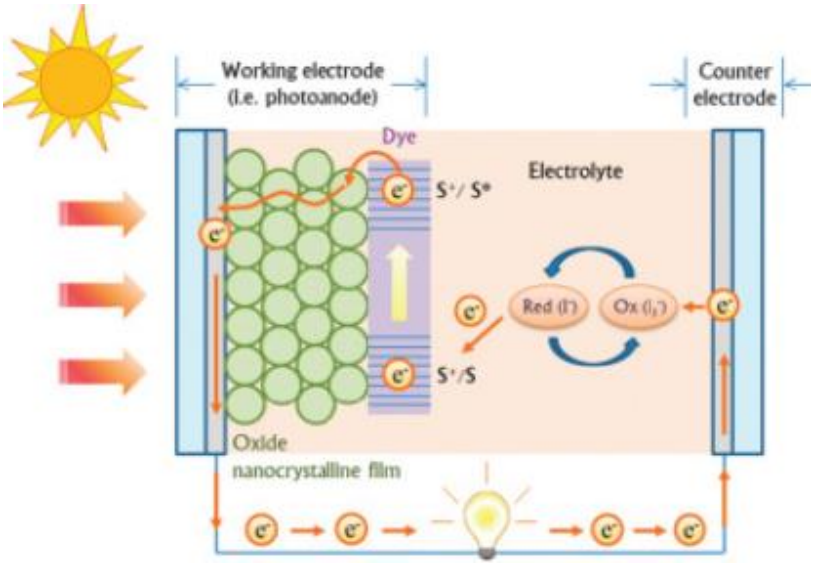

Figure 2.6: Schematic illustration of a dye-sensitized solar cell (Alagarsamy Pandikumar et al., 2016)

2.5.3.3 Quantum Dot (QD) Solar Cell

QDs are very small semiconductor particles that are several nanometres in size, their small particles make their optical and electronic properties differ from those of larger particles. Their optoelectronic properties can be modified due to their bandgaps, that are tuneable over a wide range of energy levels, by changing the dot size, this makes it attractive for multi-junction solar cells (A.Badawy, 2015). QDs also have an exceptional ability to generate multiple pairs of charge carriers with a single high-energy photon (Jasim, 2015).

In bulk semiconductors, absorption of photons with energy exceeding the bandgap promotes an electron (hot carrier) from the valance band to the higher level in the conduction band.

The excited electron (hot carrier) undergoes thermalisation or multi-phonon emission before reaching the bottom of the conduction band. However in a QD, the hot carrier undergoes an impact ionisation process or carrier multiplication (Nozik, 2002). Therefore, absorption of a single photon generates multiple electron-hole pairs called multiple exciton generation (MEG), which leads to achieving photon-conversion efficiencies greater than 100 % as absorption of UV photons in QDs produces more electrons than near infrared photons (Gail Overton, 2006; Jasim, 2015). QD structured materials can be used to create intermediate bands. Solar cells based on intermediate bandgap materials are expected to achieve maximum theoretical efficiency, as high as 65 %. This allows two sub-bandgap photons to create an electron-hole pair via a mid-gap intermediate band, refer to Figure 2.7. The intermediate energy band introduces additional photon absorption, which in turn contributes to higher photocurrent (Zheng, Ji, Yu & Wang, 2016).

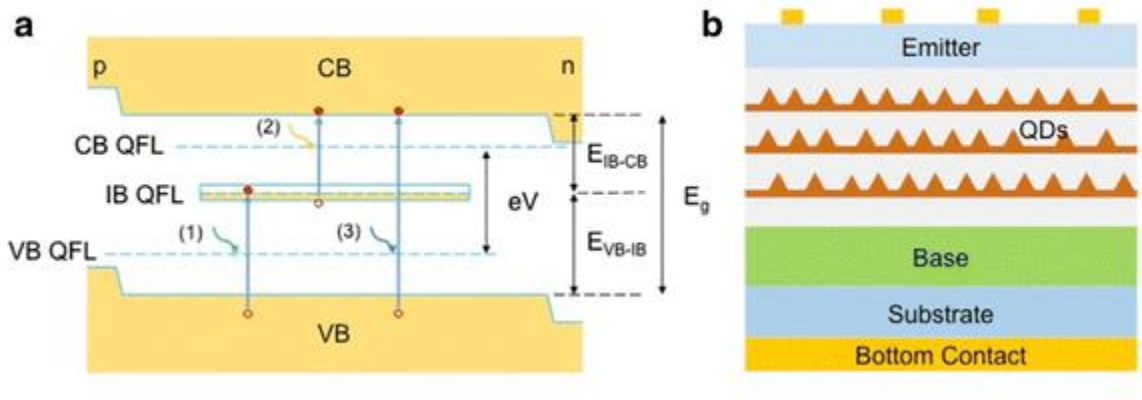

Figure 2.7: Schematic illustrations of (a) an intermediate band energy level and (b) device structure of QD-Intermediate band (Z. Zheng et al., 2016)

2.5.3.4 Tandem Solar Cells

A tandem solar cell (TSC) consists of two or more sub-cells; together they convert more of the sunlight spectrum by splitting it into multiple bands that can be efficiently

converted into electricity, thus increasing the overall cell efficiency (NREL, 2017). Each active material used to fabricate a solar cell can convert a certain wavelength of light to electricity.

To attain a better photon absorption efficiency, two or more active materials, with different bandgaps, are connected to build a TSC (Vatansever et al., 2012). The maximum efficiency of a single cell was calculated to be 30% under non-concentrated sunlight, for a tandem comprising two sub-cells with band gaps of 1.9 and 1.0 eV, the efficiency is raised to 42%. Under concentrated sunlight, the efficiencies are 40% for a single cell and 55% for a tandem with two sub-cells (Ameri et al., 2009). However, experimental studies on TSCs, consisting of dual-junction III–V/silicon cells, reached up to 32.8% efficiency under one sun illumination. An efficiency up to 35.9% was achieved for a three-junction tandem, where gallium indium phosphide/gallium arsenide (GaInP/GaAs) dual-junction cell and a silicon single-junction were combined (Essig et al., 2017), refer to Figure 2.8.

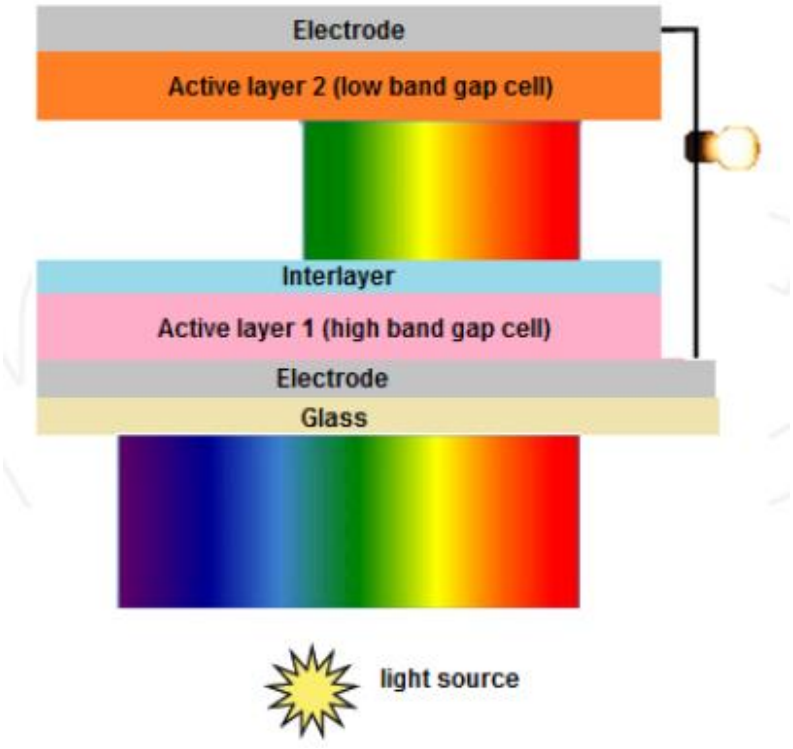

Figure 2.8: Schematic illustration of two-layer tandem junction (Vatansever et al., 2012)

2.6 Perovskite Solar Cell (PSC)

Perovskite is the name used for the mineral calcium titanate ($CaTiO_{3)}$. The crystal structure of the perovskite class of materials is represented by the formula ABX_3, where "A" and "B" are cations and "X" is an anion of different dimensions, with "A" being larger than "X", refer to Figure 2.9. Many materials which assume this structure are being used for applications based on their thermoelectric, insulating, semiconducting, piezoelectric, conducting, antiferromagnetic, and superconducting properties (Ahmed, Habib & Javaid, 2015). There are three major perovskite crystal structures: cubic, tetragonal and orthorhombic (Li, 2016).

PSC is a third-generation photovoltaic technology, the first prototype of perovskite structured material was realised with the structure of liquid DSSCs in 2009 by Kojima and his colleagues (Kojima et al., 2009). The perovskite absorber ($CH_3NH_3PbBr_3$ and $CH_3NH_3PbI_3$) replaced the conventional dye pigment in DSSCs and gained a considerable PCE of 3.13 % and 3.81 % respectively (Tang et al., 2017).

In methylammonium-based perovskite materials, A is an organic cation methylammonium ($CH_3NH_3^+$), anion X is a halogen (Cl^-, Br^-, I^-) and B is a cation (Pb^{2+}, Sn^{2+}, Eu^{2+}, Cu^{2+}). Recently, lead acetate ($Pb(Ac)_2$) precursor has been used to replace conventional lead halides (Y. Chen, Yerramilli, Shen, Zhao, & Alford, 2018; Zhao et al., 2016). The standard compound methylammonium lead triiodide ($CH_3NH_3PbI_3$), with mixed halides, $CH_3NH_3PbI_{3-x}Cl_x$ and $CH_3NH_3PbI_{3-x}Br_x$, and the use of different lead precursors like lead acetate ($Pb(Ac)_2$) are being studied for solar cell applications (Adhikari, 2016).

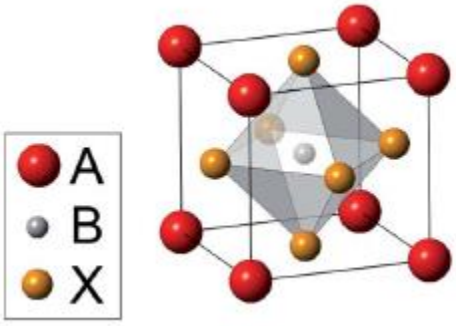

Figure 2.9: The ABX3 perovskite crystal structure (Eperon, Stranks, et al., 2014)

Recently, the methyl ammonium lead halide perovskite ($CH_3NH_3PbI_3$) has emerged as a promising photovoltaic material for the solar cell due to its excellent optical and electrical properties, such as the large light absorption coefficient (5.7×10^4 cm^{-1} at 600 nm), high charge carrier mobility (hole mobility of 164 $cm^2V^{-1}S^{-1}$ and electron mobility of 24 $cm^2V^{-1}S^{-1}$ for $CH_3NH_3PbI_3$ single-crystal perovskite), long charge diffusion length (~100 nm), and easy fabricating procedure (solution processing) (Yifan Li, 2016). PSCs have been recently researched and found that the efficiency has improved greatly from 3.8% to 22.1% (Yang et al., 2017), which indicate that perovskite will be a relevant material in photovoltaic technology. As the maximum theoretical PCE of the PSCs using $CH_3NH_3PbI_{3-x}Cl_x$ is 31.4 %, there are still possibilities of further improvement in the PCE.

2.6.1 Working Principle of PSCs and Device Structure

Perovskite layer plays the role of the active layer or light absorbing layer in the total device structure (Adhikari, 2016). Perovskite crystals absorb the light and excite electrons in the conduction band of titanium oxide (TiO_2). The electrons (charge carriers) are transported to the external circuit through the ETL and the holes left are then transported through the HTL and gather at the corresponding electrode, to form the photocurrent (Li, 2016). It was later reported that a few hundred nanometer thick solid perovskite film can sustain charge generation and is ambipolar, transporting both holes and electrons (Hsiao et al., 2015).

The device configuration for $CH_3NH_3PbI_3$-based solar cells consists of two basic structures: conventional structure (n-i-p) and inverted structure (p-i-n). The conventional structure is usually based on indium-doped titanium oxide (I_dTO) or fluorine-doped titanium oxide (F_dTO)/compact TiO_2 (ETL)/perovskite/hole-transport layer/Ag or Au (Savva, Burgués-Ceballos & Choulis, 2016). A high electrically conductive conjugated polymer poly (3,4-ethylenedioxythiophene) polystyrene sulfonate (PEDOT:PSS) or 2,2′,7,7′-tetrakis (N,N-di-4-methoxyphenylamino)-9,9′-spirobifluorene (spiro-OMeTAD) is used as the HTL on the F_dTO/I_dTO substrate. The perovskite layer, which functions as the active layer to absorb the sunlight, is usually spin coated on the surface of PEDOT:PSS or spiro-OMeTAD. On top of perovskite active layer is the ETL, whose function is transporting electrons to the cathode. The last layer cathode (silver or gold) is thermally deposited on the ETL layer (Li, 2016). The separated electrons reach the F_dTO electrode by moving from the conduction band of TiO_2 and the holes are transported to the silver electrode by moving from the valence band of Spiro-MeOTAD or PEDOT:PSS (Adhikari, 2016). For the inverted structure, the difference is the electrons and holes flow direction, the current flow is reversed by changing the polarity of the electrodes, being I_dTO or F_dTO/PEDOT:PSS/perovskite/[6,6]-Phenyl-C61-butyric acid methyl ester (PCBM)/Aluminium (Al). Usually the I_dTO or F_dTO glass is used as the cathode, with the topside layer as anode (Savva, et al., 2016).

The conventional and inverted geometries have either planar or mesoporous structure. The mesoscopic nano-structured device has a mesoporous oxide layer or scaffold layer for mechanical support, it enhances the charge collection by decreasing the carrier transport distance; thereby, increasing the absorption due to the light scattering and preventing direct leakage of current between two selective contacts (Song, Watthage, Phillips & Heben, 2016). For regular mesoporous geometry, the commonly used N-type semiconducting oxide for mesoscopic layer is TiO_2 (Jin Cui et al., 2015). TiO_2 has a wide bandgap, and is non-toxic, cheap, biocompatible and abundant. It provides mechanical support and also assists in electron transport. Al_2O_3 has also been used in the mesoscopic layer (Wojciechowski et al., 2014), because it is insulating and provides only mechanical support.

Glass/F_dTO/cp-TiO_2/mp-TiO_2/perovskite/spiro-OMeTAD/Au and Glass/F_dTO/cp-TiO_2/mp-Al_2O_3/perovskite/spiro-OMeTAD/Au are examples of conventional mesoscopic architecture (J Cui et al., 2016). Meso-superstructure concept was also evaluated with ZrO_2 mesoporous scaffold (Ahmed et al., 2015). For conventional planar geometry, the perovskite is deposited directly on compact TiO_2 layer (Glass/FTO/cp-TiO_2/perovskite/spiro-OMeTAD/Au). Although the planar n-i-p PSC usually exhibits enhanced V_{OC} and J_{SC} relative to a mesoscopic n-i-p device processed with the same materials and approach, the planar device usually exhibits more severe J−V hysteresis. As a result, the state-of-the-art n-i-p devices usually include a thin (~150 nm) mesoporous buffer layer filled and overlaid with the perovskite (Song et al., 2016), refer to Figure 2.10.

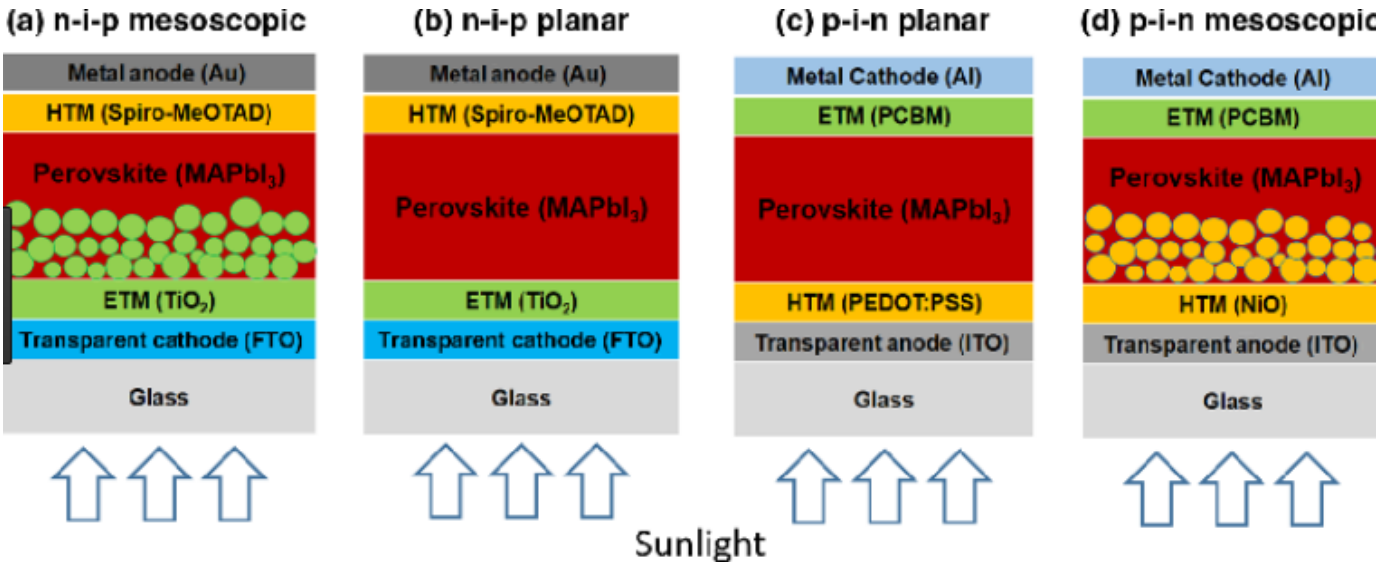

Figure 2.10: Schematic diagrams of PSCs in the (a) n-i-p mesoscopic, (b) n-i-p planar, (c) p-i-n planar, and (d) p-i-n mesoscopic structures (Song, et al., 2016)

2.6.2 Materials

For the transparent conducting electrodes, F_dTO is the most commonly used TCO for PSCs. Indium-doped titanium oxide is also used, but indium is more expensive and has low mechanical resistance (Fru, 2016). Carbon nanotubes, graphene and silver nanowires are promising materials that have been used as transparent electrodes (Rand & Richter, 2014).

2.6.2.1 Hole-Transport Materials (HTMs)

Perovskites can conduct holes, but they are present at low levels. It has been reported that a hole-conductor free mesoscopic $CH_3NH_3PbI_3/TiO_2$ heterojunction PV has a PCE of 5.5 %. This value is very low when compared to cells with HTMs and, for efficient charge extraction, an HTM layer is a necessity (Calió, Kazim, Grätzel, & Ahmad, 2016; Fan, Jia, & Gu, 2014). When the excitons dissociate into electrons and holes, the HTM transports holes to the back electrode; it reduces recombination and increases absorption (Ahmed et al., 2015).

HTMs can be organic or inorganic material. Organic HTMs include spiro-OMeTAD, poly(3-hexylthiophene) (P3HT), poly[bis(4-phenyl)(2,4,6-trimethylphenyl) (PTAA) and PEDOT: PSS (Wang, et al., 2016). Spiro-OMeTAD is the best organic HTM, in terms of performance, but it is commercially expensive and shows pinholes when the solution is processed. Spiro-OMeTAD requires an additive, namely 4-tert-butylpyridine (TBP) or bis(trifluoromethane) sulfonimide lithium salt (Li-TFSI), to improve the conductivity. However, the additives break down the perovskite layer, reducing the stability of the perovskite device (Fru, 2016; Wang et al., 2016).

Inorganic HTMs include CuI, NiO, V_2O_5, $CsSnI_3$ and copper thiocyanate. They are less expensive than organic HTMs. Inorganic oxide films display better environmental stability than organic HTMs but generally, organic HTLs have led to higher device efficiency. CuI shows very low efficiencies when used, but copper thiocyanate is a more efficient HTM for PSCs. Qin et al. incorporated copper thiocyanate with $CH_3NH_3PbI_3$ as HTMs and the device showed a PCE of 12.4% (Qin et al., 2014). Kim et al. incorporated an inorganic HTM, NiOx, which gave an efficiency of 8.94% but, when doped with copper to give (cu-NiO_x), the efficiency increased to 15.4% (Kim et al., 2015).

2.6.2.2 Electron Transport Materials (ETMs)

The ETMs transport electrons that are injected from the absorber layer (perovskite) to the electrode where they are collected.

A number of inorganic metal oxides, such as TiO_2, ZnO, SnO_2, SiO_2, ZrO_2, can either be used as ETMs or as scaffold materials (Yang et al., 2016).

The most important characteristic of an ETM is that it must satisfy band alignment with the perovskite layer, i.e. it should have LUMO and the highest occupied molecular orbital (HOMO), higher than the perovskite active layer. It must have high transmittance in the UV-Vis region so that a photon can pass through easily and be absorbed by the perovskite absorber (Mahmood, Sarwar & Mehran, 2017).

The most commonly used ETM for mesoporous PSCs is TiO_2, although oxygen vacancies and titanium interstitials can form in this layer. These defects cause deep sub-band gap trap states, which reduces solar cell performance. Oxygen is required to passivate these traps; however, other layers in the device requires encapsulation to prevent moisture entry, which degrades the solar cell (Y. Liu et al., 2016). Also, the electron injection rates from the perovskite absorber to TiO_2 ETMs are quick, but the electron recombination rates are also very high due to the low electron mobility and transport properties (Yang et al., 2016).

Pathak et al. (2014) demonstrated aluminium-doping of TiO_2 to attempt to solve this problem, which led to an increase in device performance and stability for cells with Al-doped TiO_2. ZnO nanorods and nanoparticles have both been introduced into the PSCs as ETMs, showing PCEs of 11.13% and 15.7% respectively; however, ZnO becomes chemically instable (Yang et al., 2016).

SnO_2 is another promising ETM with a wide band gap, high transparency and large electron mobility (bulk mobility: 240 $cm^2V^{-1}s^{-1}$). Li Yi., Zhu, et al. (2015) successfully utilised SnO_2 nanoparticle films as ETLs in PSCs and combined with $TiCl_4$ treatment, the efficiency of the device exceeded 10%; although, hysteresis behaviour of SnO_2-based devices needs to be addressed.

For organic ETMs, fullerene (C60) and its derivatives with different energy levels and electron mobilities, such as Phenyl-C61-butyric acid methyl ester (PC61BM), Indene-C60 Bisadduct (ICBA) and Phenyl-C71-butyric acid methyl ester (PC71BM), are usually used as efficient electron extraction materials because of their low temperature fabrication, suitable energy level alignment and decent electron mobility.

2.6.2.3 Back Contact Materials

Metal contact materials (electrodes) are needed in PSCs to collect charge carriers and deliver them to the load where power is required. They can be inorganic semiconductor/metal or organic semiconductor/metal interface depending on the structure of the solar cell (Fru, 2016). The interface between the semiconductor and the metal must be properly engineered to ensure effective collection and minimal recombination. Al, Ag, Au and carbon have been used as back contact materials on NiOx (M. Li, Shen, Wang, Guo, & Chen, 2015). Other contact materials are Ni, Cr and Si (n+). Gold is the most commonly used electrode material for high-efficiency PSCs, although it is expensive (Wang et al., 2016).

Table 2.1: Materials used as different layers in Perovskite Solar Cells (Adhikari, 2016)

Layer	Material
Cathode	Fluorine tin oxide (FTO)
Electron Transport Layer (ETL)	Compact TiO_2, mp-TiO_2
Active Layer	Perovskite ($CH_3NH_3PbI_3$)
Hole-Transport Layer (HTL)	Spiro-ometad
Anode	Silver (Ag)

2.6.3 Film Deposition Methods

There are many approaches for the synthesis of perovskite active layers, including; one-step precursor solution deposition, two-step sequential deposition, dual-source vapour deposition, vapour-assisted solution process and sequential vapour deposition.

2.6.3.1 One-step Spin-coating Method

One-step solution processing is the simplest technique for the growth of perovskite. This method involves the spin coating of a precursor solution of lead halide with a certain amount of an organic ammonium halide (Ahmed et al., 2015). Spin coating deposits uniformly-thin films on flat substrate. These rotate at high speeds (> 600 rpm), allowing the perovskite crystallites to form and grow during the solvent evaporation. A post-annealing process is carried out at a relatively high temperature (around 100^{o}C) for the complete crystallisation of the perovskite and the removal of the residual solvents. The annealing temperature, solution concentration, precursor composition and solvent choice influences the film morphology and PSC's performance (L. Zheng et al., 2015). Gamma-butyrolactone (GBL), dimethylformamide (DMF), and dimethyl sulfoxide (DMSO) are examples of solvents that are being used for the dissolution of the precursors. A mixture of solvents (DMF and GBL, DMF and DMSO, DMSO and GBL) has been used for obtaining optimum concentrations for solution processing, as higher concentrations lead to better film coverage and higher efficiency devices, owing to the rapid evaporation of this combination of solvents (Ahmed et al., 2015). Im et al. (2011) used the one-step coating method for the iodide perovskite active layer by reacting equimolar CH_3NH_2 and HI in the appropriate solvent. They then mixed the synthesised CH_3NH_3I with PbI_2 at a 1:1 molar ratio in GBL at 60^{o}C The solution was then stirred for several hours after which it was used as a coating solution.

2.6.3.2 Two-step Spin-coating Method

In a two-step deposition process, the lead salt is dissolved in DMF and deposited on the substrate, after which the lead iodide film is dried on a hot plate for 10 minutes. A solution of methyl ammonium iodide (MAI) is dissolved in isopropyl alcohol (IPA), which is used to convert the lead iodide film into perovskite (Bastiani, 2016; L. Yang et al., 2016). This conversion can be achieved in two very different ways: dipping the lead film into the MAI solution and spin coating the solution MAI on top of the lead film, or exposing the lead film to MAI vapours after which the perovskite film is annealed (Bastiani, 2016).

2.6.3.3 Dual-Source Vapour Deposition

The vapour deposition method occurs by co-evaporating the lead source and MAI in a vacuum. This makes use of vacuum technology to apply thin films of pure materials to the surface of a substrate. The crucibles containing the materials are heated to a high temperature in a vacuum (pressure < 10^{-5} Torr) using either a filament or an electron-beam (e-beam) method. The material vapourises and the vapour is transported to the target (substrate) at the top of the chamber (Sum & Mathews, 2014; L. Zheng et al., 2015); high degrees of vacuum and temperature are required, which increases the cost.

2.6.3.4 Vapour-assisted Solution Process

In the vapour-assisted solution process, the lead is deposited on the substrate by spin coating, then the MAI vapour is deposited by thermal evaporation on the pre-deposited lead source (Song et al., 2015; Zheng et al., 2015). The advantage of the thermal evaporation method is that the perovskite film can be deposited on various substrates with varied wettability and morphology. This deposition method allows better control of morphology and grain size through gas–solid crystallisation and efficiently avoids film delamination that can occur during liquid–solid interaction (Song, et al., 2016).

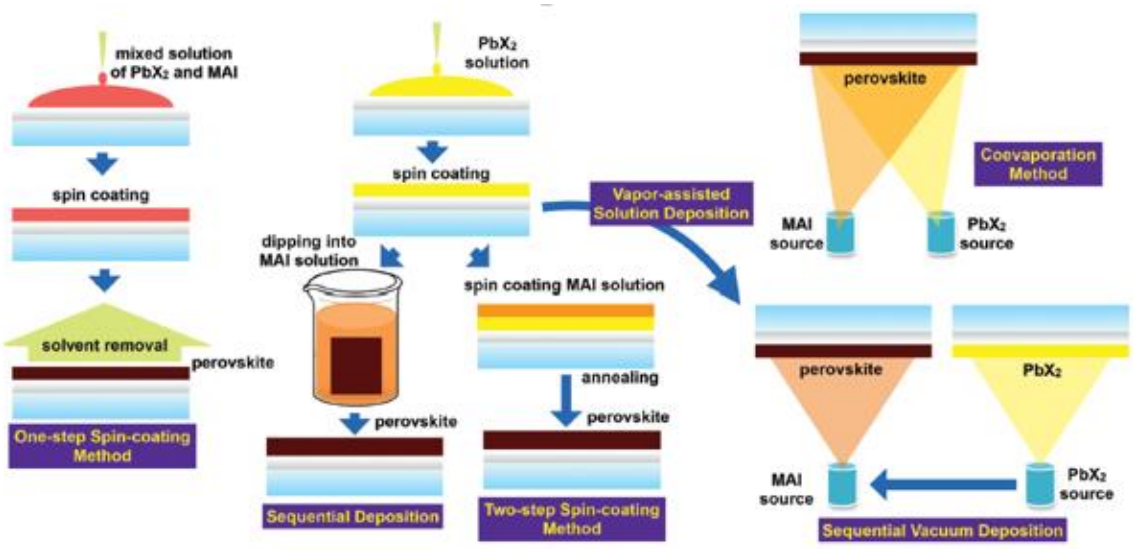

Figure 2.11: Schematic representation of different perovskite fabrication techniques (L. Zheng et al., 2015)

2.6.4 Stability of Perovskite

The stability of perovskite devices is a challenge to overcome before solar cells can be developed as commercial products. Degradation occurs when devices are exposed to thermal stress, ultraviolet (UV) light, oxygen and/or moisture (Bastiani, 2016; Yang et al., 2016). Water, due to its ionic nature, can convert the perovskite structure back to its precursor. This degradation is irreversible and occurs at the grain boundary. This is a problem for the entire life of photovoltaic cells; as PbI_2, which is a by-product of the degradation, is soluble in water and is toxic (Adhikari, 2016; Wang et al., 2016). Numerous approaches have been used to increase resistance to moisture-related degradation, including using a thin blocking layer (e.g. Al_2O_3) between the perovskite and HTM (Dong et al., 2015), the use of moisture blocking HTM (J. Liu et al., 2014) and the use of a hydrophobic carbon electrode (Asghar, Zhang, Wang, & Lund, 2017). A humidity of 55% was reported to deteriorate device efficiency, which was evident in the change in colour from dark brown to yellow (Ahmed et al., 2015). Niu, Guo and Wang (2015) suggested a sequence of chemical reactions they considered responsible for the degradation of $CH_3NH_3PbI_3$ in the presence of moisture:

$$CH_3NH_3PbI_3 \xleftrightarrow{H_2O} CH_3NH_3I_{(aq)} + PbI_2$$

$$CH_3NH_3I_{(aq)} \longleftrightarrow CH_3NH_{2(aq)} + HI_{(aq)}$$

$$4HI_{(aq)} + O_2 \longleftrightarrow 2I_{2(s)} + 2H_2O$$

$$2HI_{(aq)} \xleftrightarrow{hv} H_2\uparrow + I_{2(s)}$$

PSCs tend to degrade when light is soaked under AM1.5 G 1 sunlight, leading to a decrease in efficiency which follows the pattern of decreasing J_{SC}. The presence of TiO_2, which is photo-catalytically active for the UV light, was found to be the reason for the degradation. It was proposed that UV light should be prevented from reaching the TiO_2 layer or that the TiO_2 scaffold be replaced with another material (Asghar et al., 2017; Wang et al., 2016). Exposure to high temperatures also causes degradation of the perovskite layer. The perovskite layer therefore requires an annealing step as solar modules are inevitably subjected to high temperatures (Wang et al., 2016).

2.6.5 Morphology PSCs

The morphology of the perovskite active layer has a substantial impact on the overall performance of the solar cell. High-coverage, uniform, crystalline domains are best for achieving high power conversion efficiencies (Dualeh et al., 2014). Incomplete surface coverage, where there are pinholes and grain boundaries, may result in direct contact between electrodes or charge transport layers. This can lead to increased current leakage, induced recombination and decreased efficiency. Generally, morphology is influenced by the fabrication processes, composition of the perovskite layer, solvent, deposition method and successive post-treatments (Yang et al., 2016).

Solution deposition of planar films of the pure hybrid perovskite materials generally results in small grain size, high density of defects and low surface coverage (Zeng et al., 2017). Dual-source vacuum thermal evaporation (DSVD) and vapour-assisted solution process (VASP) are effective techniques that control crystal growth and have been used to create smooth and uniform perovskite film (Yang et al., 2016). However, thermal evaporation processes are expensive due to the high temperature and vacuum needed; therefore, processes are being improved using different methods to achieve uniform films.

2.6.6 Methods to Control the Morphology of PSCs

2.6.6.1 Solvent Engineering

Solvents have different evaporation rates and solubilise precursors with different efficiency. Various solvents and solvent additives can be used to modify the uniformity and crystallinity within a perovskite film. To control the morphology of the perovskite layer, one must understand and control the phases and the overall impurity formation in mixed halide perovskite systems, these are important for growing high quality crystals.

It is difficult to control the crystal structure of perovskite using a volatile solvent such as DMF, which has a boiling point of 153^{o}C. Higher boiling point solvents such as DMSO (189^{o}C) and GBL (204^{o}C) are usually able to create more uniform crystal domains and smoother film surfaces.

This is due to their control over the crystallinity of the inorganic PbI_2 and the subsequent reaction of PbI_2 with MAI (H-B. Kim et al., 2014). Mixed solvents have also been used to improve on film morphology. H-B. Kim et al. (2014) used a mixture of GBL and DMF (DMF:GBL 97:3 [vol%]) to create a uniform and smooth perovskite film with an efficiency of 6.16%. Jeon et al. (2014) used mixed solvents of GBL and DMSO (7:3 v/v) as a processing solvent followed by toluene drop-casting a transparent CH_3NH_3I–PbI_2–DMSO. The intermediate phase was formed first after the dropping of toluene using the GBL:DMSO blend solution. Extremely uniform and compact perovskite layers were formed after thermal annealing at 100^oC for 10 minutes (Jeon et al., 2014). Li Wenzhe, J. Fan et al. (2015) investigated the effect of mixing halide using DMF and DMSO as the precursor solvents in the two-step deposition sequence. They observed that adding DMSO to the DMF solution assisted in controlling the perovskite crystallisation, resulting in enhanced PV performance.

The application of solvents such as toluene, dichloromethane, chlorobenzene and chloroform during the spin coating of the perovskite film's surface leads to better concentration and uniform morphology. This is attributed to the rapid reduction of the solubility of $CH_3NH_3PbI_3$ in the mixed solvent, which promotes fast nucleation and crystallisation, thus leading to better crystallisation of perovskites. However, the solvent must not be able to dissolve either PbI_2 or MAI so that it cannot wash away any precursors (Xiao et al., 2016). Xiao et al. (2014) developed a fast deposition crystallisation (FDC) method using chlorobenzene (CB) to induce crystallisation during the spin-coating process. The time interval between the dripping of the process solution and that of the solvent additive is critical to obtain optimal film morphology; the best dropping time for the solvent was reported to be at the second stage, refer to Figure 2.12. Too early or too late dropping of CB cannot result in uniform and compact perovskite films.

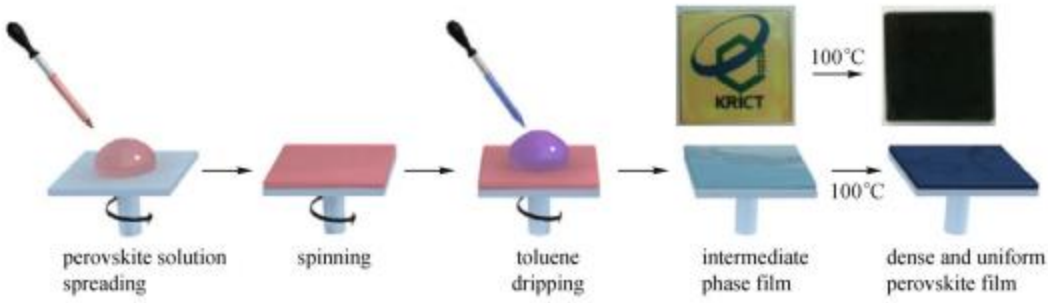

Figure 2.12: Schematic representation of solvent engineering process using toluene (Jeon et al., 2014)

2.6.6.2 Additives

Additives influence the perovskite morphology and can be added to the precursor solution. Various additives for different perovskites are mentioned in the literature. Mei et al. (2014) used 5-ammoniumvaleric acid (5-AVA) iodide in one-step solution for $CH_3NH_3PbI_3$ perovskite. Eperon, Stranks, et al. (2014) reported using hydroiodic acid (HI) as an additive for formamidinium-lead trihalide perovskite (Eperon, Stranks et al., 2014). Yang, Wang and Leung (2015) used the two-step deposition sequence for perovskite deposition, where halogen acids were added for the PbI_2 precursor solution, which promoted homogeneous nucleation and crystal growth due to the change in the crystalline PbI_2 morphology. Jeon et al. (2015) used N-cyclohexyl-2-pyrrolidone (CHP) as an additive (5% volume ratio) in the processing of the solvent DMF. Highly smooth and continuous films can be obtained by using one-step spin-coating method with 1:1 molar ratio of PbI_2 and MAI precursor solution. Chang et al. (2015) added a small amount of polyethylene glycol, which retarded the crystallisation of perovskite. By using the one-step spin-coating process, the film with 1wt% of polyethylene glycol resulted in smoother perovskite film with fewer pinholes. Another additive is 4-tert–butylpyridine (TBP), which was added to the PbI_2 precursor solution in the two-step deposition sequence, it also improved the perovskite film morphology (Cohen & Etgar, 2016).

2.6.6.3 Thermal Annealing

Another parameter controlling perovskite morphology is the annealing of the perovskite film, which can be performed at various temperatures. It is the most applied technique to increase the crystallinity of materials, especially thin films, because of its simplicity. It has been utilised to modify the morphology of the perovskite film prepared by both one-step and two-step methods (Xiao et al., 2016). Thermal annealing functions include: (1) assisting the formation of perovskite and enhancing its crystallinity and grain growth, and (2) assisting the evaporation of the excess amount of MAI and by-products (Zhang et al., 2015).

Both annealing temperature and duration are crucial for the best film quality: excessively high annealing temperatures are able to grow large perovskite grains, but tend to reduce the surface coverage, cell efficiency and eventually decomposition of the perovskite layer (L. Yang et al., 2016). Eperon, Burlakov, et al. (2014) observed that, for the one-step deposited perovskite film on compact TiO_2 using 3:1 molar ratio of MAI to PbCl2, as annealing temperature or duration increased, the surface coverage reduced. The reported methods of thermal annealing include pre-annealing, post-annealing, low-pressure vapour annealing, multi-step annealing, multiple annealing (Zeng et al., 2017).

Moore et al. (2014) formed perovskite films at 100^{o} C using lead chloride ($PbCl_2$) and lead acetate ($PbAc_2$) as lead sources and MAI as the organic precursor. It took around 2.5 min and 43.8 min, respectively, for all the by-product to evaporate from the film since methyl ammonium acetate (MAAc) has higher volatility than methyl ammonium chloride (MACl). However, the perovskite did not form at 100^{o}C using PbI_2 as the lead source, even after 12 hours of annealing. It needed a temperature of 150^{o}C and took 17.8 min for all the by-products (MAI) to evaporate. Hsu et al. (2014) used a two-step annealing technique, first annealing at 90^{o}C for 30 minutes followed by a second anneal at 100^{o}C for 2 minutes and found that a more continuous and crystalline film was created than annealing at 100^{o}C for 5 minutes.

Dualeh et al. (2014) investigated the effect of annealing temperatures used in the conversion process to form perovskite from the deposited precursor solution. They demonstrated that a minimum temperature of 80^{o}C is required to form the $CH_3NH_3PbI_3$ perovskite. However, they found that devices performed best when fabricated between 80^{o}C and 100^{o}C.

2.6.7 Previous Works on Perovskite

Kojima et al. (2009) were the first to report on the photovoltaic results of perovskites; they were attracted by the self-organisation potential of perovskite in the nanoporous TiO_2 layer of dye-sensitised cells. In 2011, Im and colleagues used similar structures in which perovskite was shown to be deposited as sparsely spaced hemispherical nanoparticles that were approximately 2.5 nm in diameter; by applying TiO_2 surface treatment prior to deposition, they realised an efficiency of 6.5% (Im, Lee, Lee, Park & Park, 2011). In 2012, Kim et al. used spiro-MeOTAD and mesoporous (mp)-TiO_2 as the hole-transport (HTM) and electron transport (ETM) materials and obtained a PCE of 9.7% for the first reported perovskite-based solid-state mesoscopic heterojunction solar cell (Kim H-S et al., 2012). In 2012, Lee et al. replaced mesoporous TiO_2 with mesoporous aluminium oxide (Al_2O_3) and achieved an efficiency of 10.9% (Lee, Teuscher, Miyasaka, Murakami & Snaith, 2012).

Burschka and colleagues reported an efficiency of 12.0% when they used a solid perovskite capping layer overlaying the scaffolding: nanoporous TiO_2 infiltrated by perovskite (Burschka et al., 2013). Burschka used TiO_2 scaffolding and two-step iodide deposition, which improved with a confirmed efficiency of 14.1%. Liu et al. fabricated planar structured PSCs with a vapour-deposited perovskite layer and obtained PCE over 15% with an open-circuit voltage of 1.07 V without using mesoporous layers (M. Liu, Johnston, & Snaith, 2013). In 2014, Zhou et al. achieved an efficiency of 19.3% by fabricating PSC under controlled humidity conditions (30% ~5% relative humidity) with solution processing (Zhou et al., 2014). In 2015, Yang et al. achieved an efficiency of 20.2% using formamidinium-lead iodide ($FAPbI_3$), which has broad absorption compared to conventional methyl ammonium lead iodide (Yang W. S. et al., 2015).

In 2016, Saliba and colleagues showed a stabilised efficiency of 21.1% and18 % after 250 hours under standard operational conditions; they used a mixture of Cs/$MAPbI_3$/$FAPbI_3$ cation, indicating that adding caesium to $MAPbI_3$/$FAPbI_3$ induced uniform perovskite grains (Saliba et al., 2016).

At present, the efficiency of PSC is 22.1%, which was achieved by Yang and colleagues, through iodide management in formamidinium-lead-halide-based perovskite layers (Yang et al., 2017). Watthage et al. investigated the nucleation and growth of methyl ammonium lead iodide perovskite formed by reacting pre-deposited PbI_2 thin films with different concentrations of MAI solution, where they proposed that formation of perovskite films is determined by MAI concentration (Watthage, Song, Liyanage, Phillips & Heben, 2016). Eperon, Burlakov, et al., (2014) demonstrated that the highest photocurrents are determined with the highest perovskite surface coverages; which is achieved by carefully controlling the morphology, through varying the process conditions.

Zhang et al. (2015) prepared PSCs with lead acetate $Pb(CH_3COO)_2$ ($Pb(OAc)_2$) as a precursor and obtained smooth, pinhole-free perovskite films on TiO_2/FTO/glass substrates; which gave devices the power conversion of 15.2%. Li Cong et al. (2017) prepared a planar heterojunction PSC from ($Pb(OAc)_2$) through one-step spin coating, the films derived showed enhanced surface coverage and improved photoluminescence, which gave a PCE of 14.1%. In 2016, Zhao et al. demonstrated a strategy to improve the efficiency of lead acetate-based PSC by using methyl ammonium bromide as an additive in the ($Pb(OAc)_2$) and MAI precursor solution, resulting in uniform, compact and pinhole-free perovskite films with an output efficiency of 17.6% (Zhao et al., 2016). Chen et al. (2018) prepared PSC using ($Pb(OAc)_2$) and MAI as source materials, and a suitable amount of excessive ($Pb(OAc)_2$), about 5 mol% excessive Pb in the solution made the film smoother with improved film crystallinity and PCE of nearly 14%.

Table 2.2: Previous works on PSC and the improvements on its efficiency

AUTHOR	YEAR	METHOD	PCE (%)
Park et al.	2011	Deposited perovskite as hemispherical nanoparticles using TiO_2 surface treatment prior to deposition	6.5
Kim et al.	2012	Used spiro-MeOTAD and mesoporous (mp)-TiO_2 as the HTM and ETM	9.7
Lee et al.	2012	Replaced mesoporous TiO_2 with mesoporous Aluminium Oxide (Al_2O_3)	10.9
Grätzel et al.	2013	Used a solid perovskite capping layer overlying the scaffolding, nanoporous TiO_2 infiltrated by perovskite	12.0
Burschka et al.	2013	Used TiO_2 scaffolding and two-step iodide deposition	14.1
Snaith et al.	2013	Fabricated planar structured PSCs with vapour-deposited perovskite layer	15
Zhou et al.	2014	Fabricated PSC under controlled humidity conditions (30% ~5% relative humidity) with solution processing	19.3
Yang et al.	2015	Used formamidinium-lead iodide ($FAPbI_3$), which has broad absorption compared to conventional methyl ammonium lead iodide	20.2
Saliba et al.	2016	Used mixture of Cs/$MAPbI_3$/$FAPbI_3$ cation, it was shown that adding caesium to $MAPbI_3$/$FAPbI_3$ induced uniform perovskite grains	21.1
Seok et al.	2017	Used iodide management process in formamidinium-lead-halide–based perovskite layers	22.1

CHAPTER THREE: EXPERIMENTAL PROCEDURE

3.1 Equipment

The following equipment was used for this experimental work:

- Weighing balance
- Spin-coating machine
- Scanning electron microscope
- UV/VIS Spectrophotometer
- X-ray Diffractometer (XRD)
- Hot plate
- Tweezers

3.2 Chemicals

The following chemicals were used for this experimental work:

- Methyl ammonium lead iodide (Sigma Aldrich, 99.99%)
- Lead (II) iodide (Sigma Aldrich, 99.99%)
- Lead acetate trihydrate ($Pb(OAc)_2.3H_2O$) (Alfa Aesar)
- N,N-Dimethylformamide (DMF)
- Isopropanol
- Acetone
- Ethanol
- Deionised water.

3.3 Experimental Method

3.3.1 Lead Iodide Source Perovskite

The glass slides were cleaned in detergent for 15 minutes; afterwards they were rinsed with deionised water. The washed glass slides were placed in acetone for 30 minutes, followed by 30 minutes in ethanol, at room temperature. The glass slides were allowed to dry at room temperature. Perovskite $CH_3NH_3PbI_3$ films were prepared using the two-step spin-coating technique.

$PbI_2 + CH_3NH_3I \rightarrow CH_3NH_3PbI_3$ *Equation 5*

3.3.2 Two-step Spin-coating Process

460 mg PbI_2 was dissolved in 1ml DMF and stirred at 80^oC for 5 hours to obtain a transparent yellow solution. MAI (CH_3NH_3I) solution was prepared by dissolving 30 mg CH_3NH_3I in 1ml IPA for 30 minutes. The PbI_2 solution was spin coated on a glass substrate using a two-step speed; 1000 rpm for 10 seconds followed by 4000 rpm for 20 seconds then thermally annealed at 85^o C for 10 minutes. The MAI solution was spin coated onto PbI_2 film at a speed of 4000 rpm for 30 seconds. Finally, the films were heated at 100^oC for 60 minutes to remove residual IPA and the films changed from yellow to dark brown.

3.3.3 Lead Acetate Source Perovskite

3.3.3.1 Anhydrous Lead Acetate

To prepare the perovskite precursor solution, 477 mg MAI and 325 mg $Pb(OAc)_2$ were dissolved in 1 ml anhydrous DMF solution. The $Pb(OAc)_2$:MAI solutions were then spin coated for 60 seconds on the glass substrate at 4000 rpm using the one-step spin-coating method, followed by thermal annealing at 90^oC for 5 minutes, resulting in perovskite films with a thickness of about 250 nm.

This is the equation leading to the preparation of solution:

$Pb(CH_3COO)_2 + 3CH_3NH_3I \rightarrow CH_3NH_3PbI_3 + 2CH_3NH_3CH_3COO\uparrow$ Equation 6

3.3.3.2 Lead Acetate Trihydrate

379 mg of lead acetate trihydrate ($Pb(OAc)_2.3H_2O$) and 477 mg of MAI were dissolved in 1 ml of DMF. The solution was spin coated on the glass substrate at the rate of 4000 rpm for 60 seconds before annealing on the hot plate at 80^oC for 15 minutes. This process was repeated but annealing was done at a temperature of 90^oC for 15 minutes.

Lead iodide, MAI and 5% lead acetate (trihydrate) were also dissolved in 1 ml of DMF, the solution was spin coated on the glass substrate at the rate of 4000 rpm for 30 seconds before annealing on a hot plate at 100^{o}C for 1 hour.

3.4 Characterisation

The perovskite films formed were analysed to study their morphology. SEM (SEM-XL30 Environmental FEG (FEI)) was used to examine the surfaces and provide a cross section of the perovskite films. X-ray diffraction (XRD) measurements were conducted to investigate the nature of the material formed, the phase composition and the crystalline quality of perovskite thin films, the XRD measurements were done with an X-ray diffractometer using Cu Kα radiation at a step of 0.01^{o}. A Cary 5000 UV/VIS spectrometer was used to measure the optical absorption and transmittance spectrum of the perovskite film.

CHAPTER FOUR: RESULTS AND DISCUSSION

4.1 X-Ray Diffraction (XRD)

Figure 4.1 shows the XRD analysis of the perovskite films, using lead acetate and lead iodide precursors. A series of diffraction peaks appear in the five different samples of perovskite films, which indicates the formation of perovskite film when using different lead precursors. Figure 4.1A shows the analysis of lead iodide-based perovskite film, PbI_2 peak can be seen at a position of 12.68^o and perovskite peaks at 14.16^o and 28.55^o, which are assigned to the (110) and (220) planes of perovskite crystal; the observed peaks agree with previous reports (Zhao et al., 2016; Zuo et al., 2016). The presence of PbI_2 peaks indicates that it was not used up completely in its reaction with MAI and the conversion to perovskite film was incomplete. This was also observed by Aldibaja et al. (2015), where traces of PbI_2 were formed in the perovskite film and the peak was reduced when $Pb(NO_3)_2$ was used as a lead precursor. Anhydrous lead acetate was used as a precursor, which reduced the intensity of the unreacted lead with a peak at 11.5^o and perovskite peaks at 14.1^o and $28.4^{o,}$ as shown in Figure 4.1B. When lead trihydrate ($Pb(OAc)_2.3H_2O$) precursor was used, after annealing at 80^oC for 15 minutes, perovskite films were formed with very little trace of PbI_2 at 12.6^o, as seen in Figure 4.1C. Another sample was prepared using $Pb(OAc)_2.3H_2O$; however, annealing was done at 90^oC for 15 minutes, and the perovskite film was completely formed with no trace of PbI_2 (Figure 4.1D). This demonstrates that annealing temperatures influences the quality of the perovskite film formed (Dualeh et al., 2014)(Li Cong et al., 2017). The presence of PbI_2 in perovskite film leads to the degradation of the perovskite layer (Chen et al., 2018). In order to improve the perovskite film fabricated using PbI_2, 5% of lead trihydrate was added to lead iodide (Figure 4.1E); this reduced the intensity of the PbI_2 peak compared to when only PbI_2 was used. $Pb(OAc)_2.3H_2O$ has potential in fabricating perovskite films, as can clearly be seen in Figure 4.1F, there was no trace of any unreacted PbI_2 diffraction peaks.

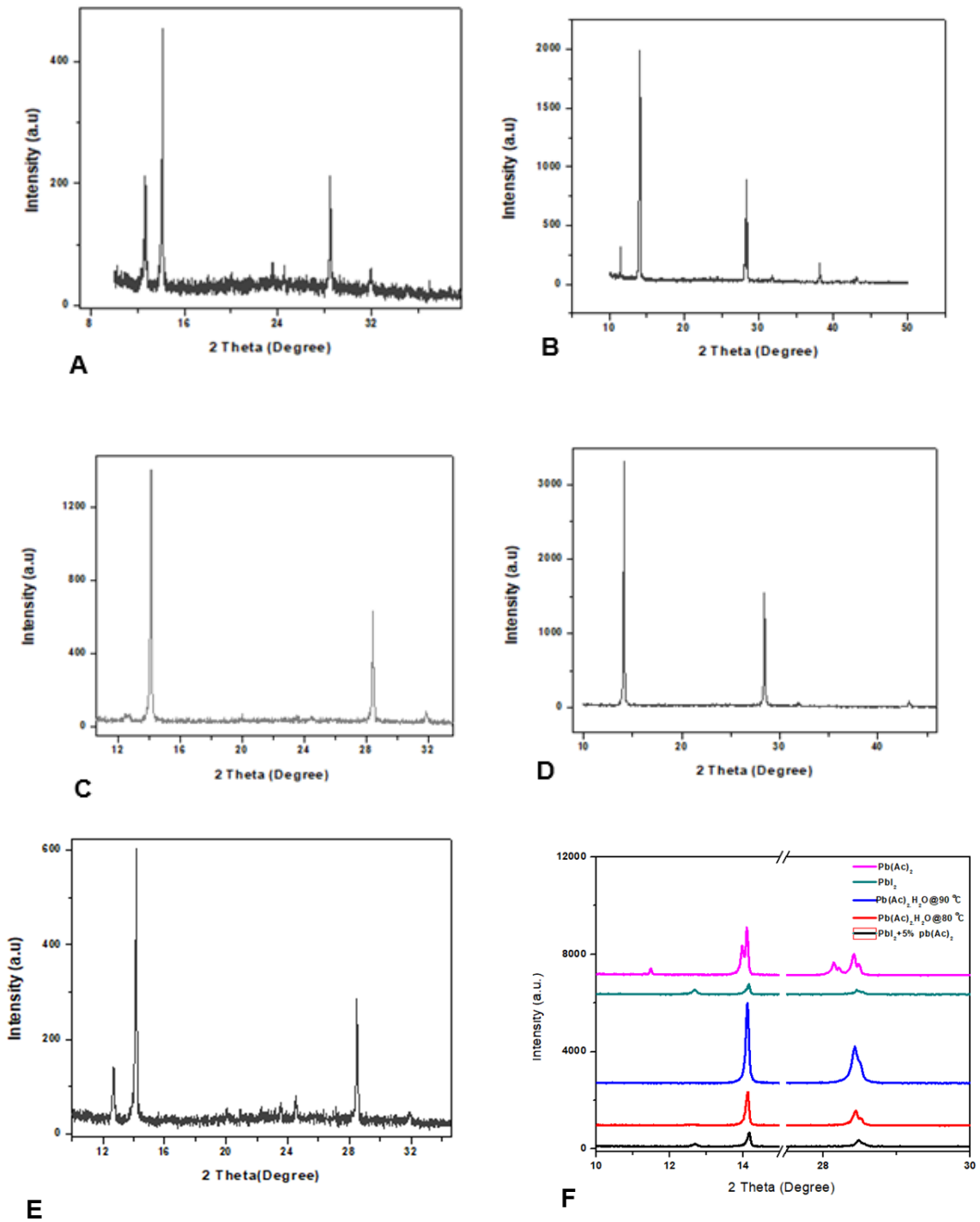

Figure 4.1: X-ray diffraction pattern of perovskite layer from (A) PbI2; (B) Pb(Ac)2 source; (C) Pb(Ac)2.3H2O annealed at 80 ^{o}C; (D) Pb(Ac)2.3H2O annealed at 90 ^{o}C; (E) PbI2 + 5% Pb(Ac)2; (F) different lead source composition

4.2 Ultraviolet-Visible Light (UV-VIS) Spectrometry

Optical absorption measurements were taken in order to monitor the band edge transition of the perovskite films formed. Figure 4.2 shows the absorbance of the different perovskite samples, perovskite film that was fabricated from PbI_2 did not show any remarkable absorption, refer to Figure 4.2A. However, perovskite fabricated using both anhydrous and hydrated lead acetate had strong broad absorption, which is evident around 750 nm in Figures 4.2B, C and D. This shows that perovskite derived from $Pb(OAc)_2$ has a stronger absorbance of the entire spectrum than PbI_2-derived perovskite film.

The absorption shoulder, which is evident at 750 nm, is as a result of the direct gap transition from the first valence band maximum to the conduction band minimum (Xu et al., 2016). The strong light harvesting capacity could be as a result of the quality of the perovskite crystals fabricated from $Pb(OAc)_2$, the results obtained are in line with previous reports (Li Cong et al., 2017).

The perovskite film formed by adding 5% lead trihydrate to lead iodide did not influence the light harvesting capacity of the perovskite as there was no obvious improvement on the absorption curve (Figure 4.2E). The result shows that lead acetate is a better precursor in fabricating perovskite as it has a stronger light absorbance capacity.

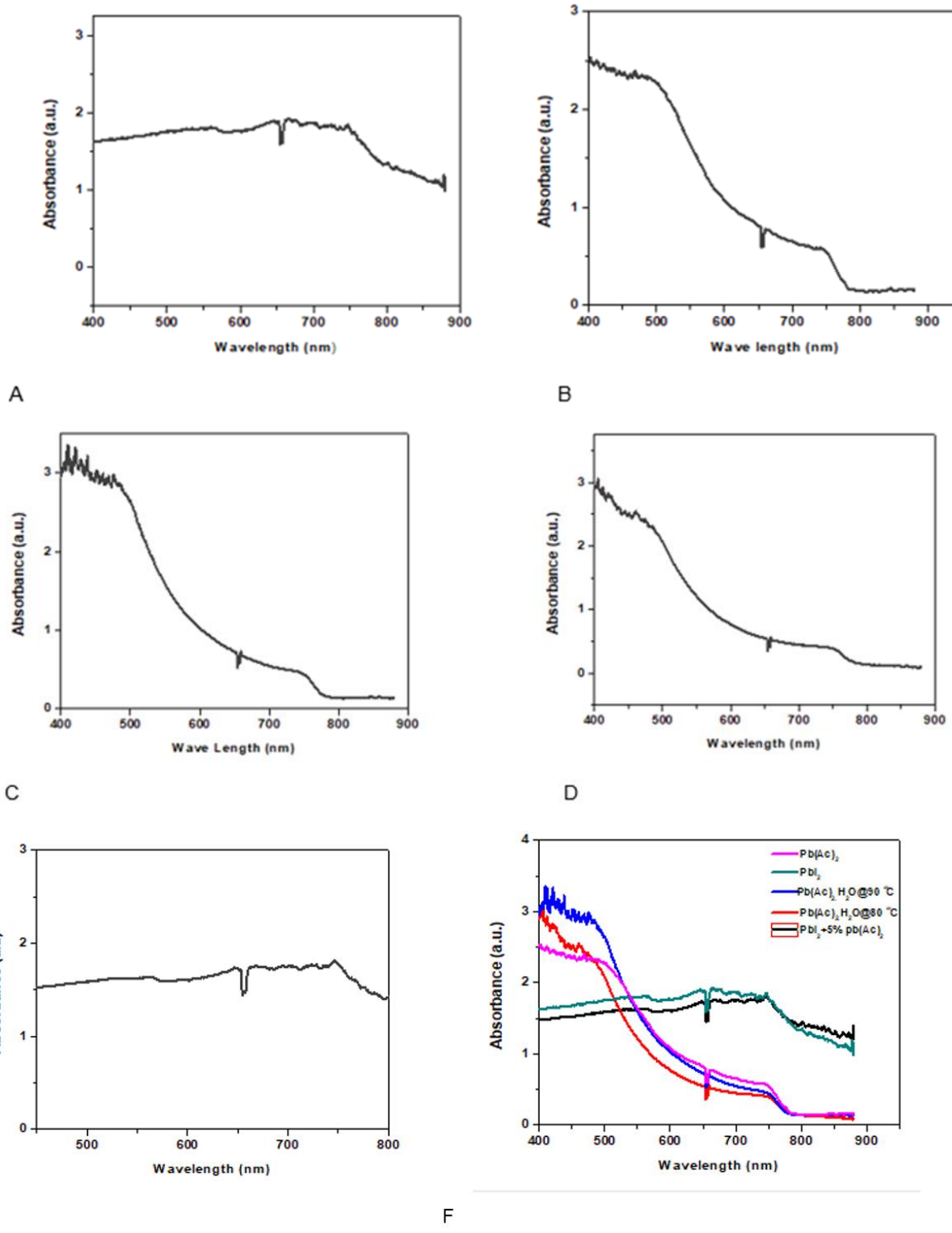

Figure 4.2: UV-VIS absorption spectra of perovskite layer from (A) PbI2; (B) Pb(Ac)2 source; (C) Pb(Ac)2.3H2O annealed at 80 ^{o}C; (D) Pb(Ac)2.3H2O annealed at 90 ^{o}C; (E) PbI2 + 5% Pb(Ac)2; (F) different lead source composition

4.3 Scanning Electron Microscopy (SEM)

The surfaces of the fabricated perovskite films were observed using the SEM, as shown in Figure 4.3. Perovskite film fabricated from PbI_2 precursor had many pinholes and a rough surface (Figure 4.3A). The crystals formed are needle-like in appearance, possibly a result of the poor perovskite crystals formed, which is in line with what Li Yahui et al. (2017) observed when they used a lead iodide source with a low concentration of MAI in the preparation of perovskite films. Perovskite films from anhydrous $Pb(OAc)_2$ had a smoother surface with no pinholes and made of larger grains (Figure 4.3B), compared to perovskite films made from hydrated $Pb(OAc)_2$ (Figures 4.3C and D). The perovskite fabricated from $Pb(OAc)_2.3H_2O$ annealed at 80^oC for 15 minutes (Figure 4.3C) had a smoother surface with no pinholes compared to $Pb(OAc)_2.3H_2O$-based perovskite annealed at 90^oC for 15 minutes (Figure 4.3D) which had very few pinholes. This shows that annealing temperature influences the smoothness of the surface of fabricated perovskites. Dualeh et al. (2014) made the same observation when, at higher annealing temperatures, the perovskite films formed were rougher with pinholes. The $Pb(OAc)_2$-based perovskite had a better morphology than the PbI_2-based perovskite because it has more volatile by-products due to its melting point, which is 280^o C, compared to 402^oC for PbI_2; hence the annealing time for $Pb(OAc)_2$ is reduced to 15 minutes compared to 60 minutes for PbI_2. According to Dualeh et al. (2014), formation of the perovskite films, which consist of solvent vapourisation, perovskite crystallisation and the sublimation of excess organic product, needs to take place. These processes occur concurrently and their occurring rates determine the composition of the final film and contribute to the different film morphologies seen in the SEM images. The 5% $Pb(OAc)_2.3H_2O$ added to the PbI_2-based perovskite did not have any remarkable influence on the morphology of the perovskite film formed, as evident in Figure 4.3E. A perovskite absorption layer derived from anhydrous lead acetate has a better morphology; hence it can improve the efficiency of perovskite-based solar cells when used as a precursor.

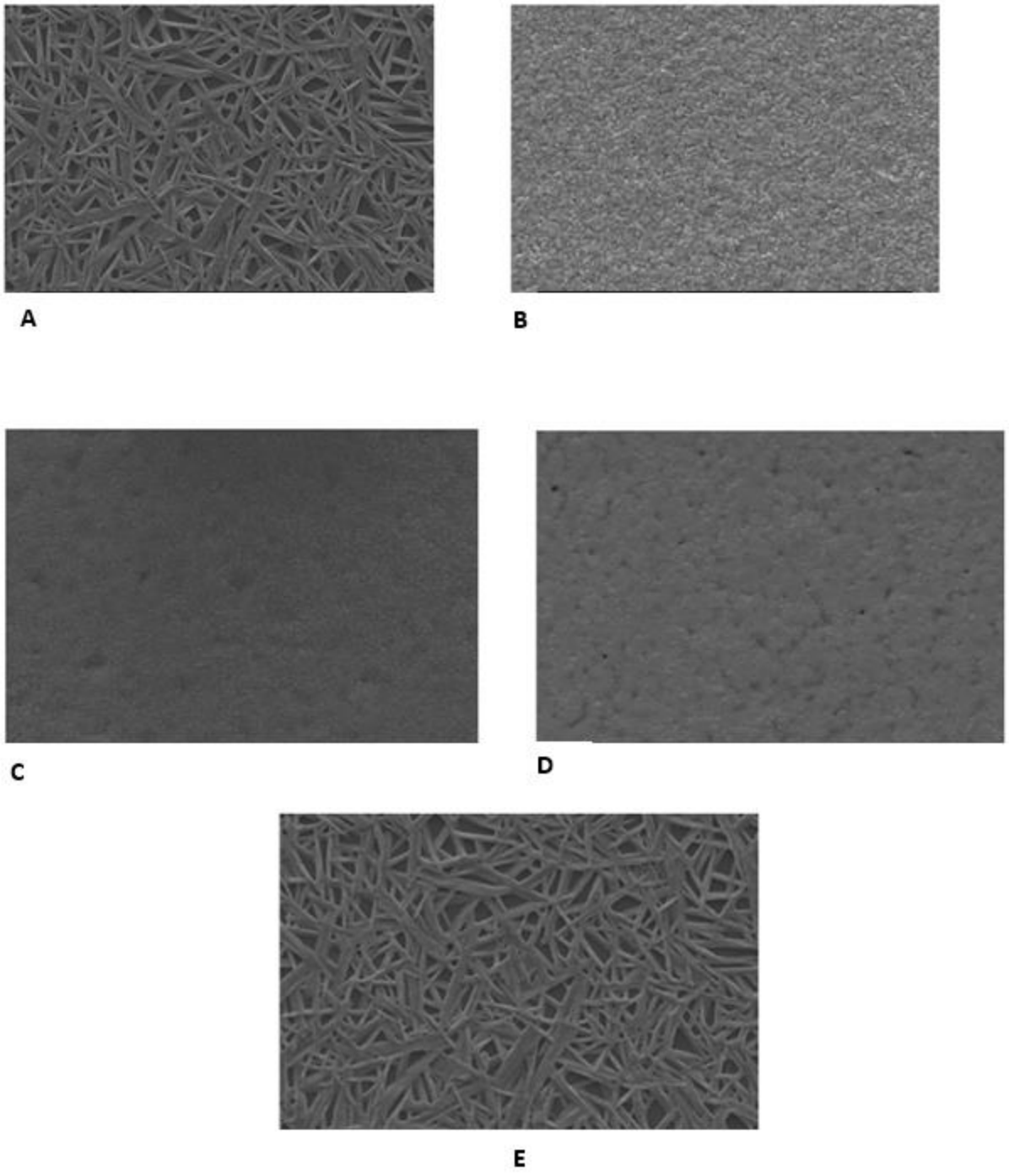

Figure 4.3: SEM images of perovskite layer from (A) PbI2; (B) Pb(Ac)2 source; (C) Pb(Ac)2.3H2O annealed at 80 ^{o}C; (D) Pb(Ac)2.3H2O annealed at 90 ^{o}C; (E) PbI2 + 5% Pb(Ac)2

CHAPTER FIVE: CONCLUSION

5.1 Introduction

In this work, perovskite films were prepared using two different lead sources; $Pb(CH_3COO)_2$ ($Pb(OAc)_2$) and PbI_2, with CH_3NH_3I (MAI) as precursor materials. The structural, optical and absorbance properties of the perovskite films varied with the lead sources used. The perovskite film derived from hydrated lead acetate showed enhanced surface coverage, uniform and pinhole-free morphology and high crystallinity in comparison to PbI_2-sourced perovskite film. It was observed that the morphology of perovskite films is strongly influenced by the lead precursor used and the annealing temperature. This is because perovskite film from $Pb(OAc)_2.3H_2O$ annealed at 90^oC gave a smoother film compared to the film annealed at 80^oC. It was also observed that when 5% of lead trihydrate was added to lead iodide in the precursor solution, it improved the perovskite film fabricated. These results indicate that lead acetate can achieve a highly efficient perovskite film for solar cells application.

5.2 Recommendations

For the purpose of further research and development, the following recommendations are proposed:

A complete solar cell device can be built on a flexible substrate, using the results from this work, to analyse the PCE, to investigate its morphology and efficiency for a wider range of applications. So far, it has been established, through research, that the efficiency of lead iodide-based perovskite is higher than lead acetate perovskite, more molar percentage (greater than 5% mols) of lead acetate can be varied and added to lead iodide in solution, the investigation should be carried out for improved morphology and efficiency.

The investigation can be carried out to study life expectancy of perovskite films and the degradation mechanisms of perovskite films fabricated from different lead sources.

More characterisation analysis can be carried out on fabricated PSC using Raman spectroscopy to further analyse the structure of the cell. Due to its sensitivity to structural changes in the molecular framework of a material, it will provide the laterally resolved microstructural information of the perovskite cell.

REFERENCES

A.Badawy, W. (2015). A review on solar cells from Si-single crystals to porous materials and quantum dots. *Journal of Advanced Research*, *6*(2), 123–132. https://doi.org/10.1016/J.JARE.2013.10.001

Adhikari, N. (2016). Nanoscale Study of Perovskite Solar Cells for Efficient Charge Transport.

Ahmed, M. I., Habib, A., & Javaid, S. S. (2015). Perovskite Solar Cells : Potentials , Challenges , and Opportunities. *International Journal of Photometry*, *2015*, 1–13. https://doi.org/10.1155/2015/592308

Alagarsamy Pandikumar, Su-PeiLim, SubramaniamJayabal, Nay Ming Huang, Hong Ngee Lim, & RamasamyRamaraja. (2016). Titania@gold plasmonic nanoarchitectures: An ideal photoanode for dye-sensitized solar cells. *Renewable and Sustainable Energy Reviews*, *60*, 408–420. https://doi.org/10.1016/J.RSER.2016.01.107

Alternative Energy. (2017). Solar Cell I-V Characteristic and Solar I-V Curves. Retrieved October 10, 2017, from http://www.alternative-energy-tutorials.com/energy-articles/solar-cell-i-v-characteristic.html

Ameri, T., Dennler, G., Lungenschmied, C., & Brabec, C. J. (2009). Organic tandem solar cells: A review. *Energy & Environmental Science*, *2*(4), 347. https://doi.org/10.1039/b817952b

American Chemical Society. (2014). How a Solar Cell Works. Retrieved October 2, 2017, from https://www.acs.org/content/acs/en/education/resources/highschool/chemmatters/past-issues/archive-2013-2014/how-a-solar-cell-works.html?cq_ck=1396892718960

Asghar, M. I., Zhang, J., Wang, H., & Lund, P. D. (2017). Device stability of perovskite solar cells – A review. *Renewable and Sustainable Energy Reviews*, *77*(July 2016), 131–146. https://doi.org/10.1016/j.rser.2017.04.003

Bae, S., Park, J.-S., Han, I. K., Shin, T. J., & Jo, W. H. (2017). CH 3 NH 3 PbI 3 crystal orientation and photovoltaic performance of planar heterojunction perovskite solar cells. *Solar Energy Materials and Solar Cells*, *160*(June 2016), 77–84. https://doi.org/10.1016/j.solmat.2016.10.019

Bagher, A. M. (2014). Introduction to Organic Solar Cells. *Sustainable Energy*, *2*(3), 85–90. https://doi.org/10.12691/RSE-2-3-2

Baghzouz, Y. (2017). Photovoltaic Devices II The p-n junction diode. Retrieved October 10, 2017, from http://www.egr.unlv.edu/~eebag/Photovoltaic Devices II-new.pdf

Bailie, C. D., Christoforo, M. G., Mailoa, J. P., Bowring, A. R., Unger, E. L., Nguyen, W. H., … McGehee, M. D. (2015). Semi-transparent perovskite solar cells for tandems with silicon and CIGS. *Energy Environ. Sci.*, *8*(3), 956–963. https://doi.org/10.1039/C4EE03322A

Bastiani, M. De. (2016). Ph . D . Thesis : The stability of third generation solar cells Università degli Studi di Padova, (October).

Bella, F., Griffini, G., Correa-Baena, J.-P., Saracco, G., Gratzel, M., Hagfeldt, A., … Gerbaldi, C. (2016). Improving efficiency and stability of perovskite solar cells with photocurable fluoropolymers. *Science*, *354*(6309), 203–206. https://doi.org/10.1126/science.aah4046

Calió, L., Kazim, S., Grätzel, M., & Ahmad, S. (2016). Hole-Transport Materials for Perovskite Solar Cells. *Angewandte Chemie International Edition*, *55*(47), 14522–14545. https://doi.org/10.1002/anie.201601757

Chen, F. (2015). Characterization and application of Pb-based organometal halide perovskite. *Thesis Cagliari Univ.*

Chen, Y., Yerramilli, A., Shen, Y., Zhao, Z., & Alford, T. (2018). Effect of excessive Pb content in the precursor solutions on the properties of the lead acetate derived CH 3 NH 3 PbI 3 perovskite solar cells. *Solar Energy Materials and Solar Cells*, *174*, 478–484. https://doi.org/10.1016/j.solmat.2017.09.039

Chritiana Honsberg, & Stuart Bowden. (2017a). Short-Circuit Current | PVEducation. Retrieved October 10, 2017, from http://www.pveducation.org/pvcdrom/short-circuit-current

Christiana Honsberg, & Stuart Bowden. (2017b). Solar cell fill factor. https://doi.org/10.1016/0038-1101(81)90062-9

Christiana Honsberg, & and Stuart Bowden. (2017c). Solar Cell Efficiency | PVEducation. Retrieved November 9, 2017, from http://www.pveducation.org/pvcdrom/solar-cell-efficiency

Cohen, B.-E., & Etgar, L. (2016). Parameters that control and influence the organo-metal halide perovskite crystallization and morphology. *Frontiers of Optoelectronics*, *9*(1), 44–52. https://doi.org/10.1007/s12200-016-0630-3

Cui, J., Yuan, H., Li, J., Xu, X., Shen, Y., & Lin, H. (2016). Recent progress in efficient hybrid lead halide perovskite solar cells. *And Technology of ….*

Cui, J., Yuan, H., Li, J., Xu, X., Shen, Y., Lin, H., & Wang, M. (2015). Recent progress in efficient hybrid lead halide perovskite solar cells. *Science and Technology of Advanced Materials*, *16*(3), 036004. https://doi.org/10.1088/1468-6996/16/3/036004

Dong, X., Fang, X., Lv, M., Lin, B., Zhang, S., Ding, J., & Yuan, N. (2015). Improvement of the humidity stability of organic–inorganic perovskite solar cells using ultrathin Al $_2$ O $_3$ layers prepared by atomic layer deposition. *Journal of Materials Chemistry A*, *3*(10), 5360–5367. https://doi.org/10.1039/C4TA06128D

Dualeh, A., Tétreault, N., Moehl, T., Gao, P., Nazeeruddin, M. K., & Grätzel, M. (2014). Effect of annealing temperature on film morphology of organic-inorganic hybrid pervoskite solid-state solar cells. *Advanced Functional Materials*, *24*(21), 3250–3258. https://doi.org/10.1002/adfm.201304022

Eperon, G. E., Burlakov, V. M., Docampo, P., Goriely, A., & Snaith, H. J. (2014). Morphological control for high performance, solution-processed planar heterojunction perovskite solar cells. *Advanced Functional Materials*, *24*(1), 151–157. http://doi.org/10.1002/adfm.201302090

Eperon, G. E., Stranks, S. D., Menelaou, C., Johnston, M. B., Herz, L. M., & Snaith, H. J. (2014). Formamidinium lead trihalide: a broadly tunable perovskite for efficient planar heterojunction solar cells. *Energy & Environmental Science*, *7*(3), 982. https://doi.org/10.1039/c3ee43822h

EPIA, & GreenPeace. (2006). *Solar Generation:Solar Electricity for over one billion people and two million jobs by 2020.*

Essig, S., Allebé, C., Remo, T., Geisz, J. F., Steiner, M. A., Horowitz, K., … Tamboli, A. (2017). Raising the one-sun conversion efficiency of III–V/Si solar cells to 32.8% for two junctions and 35.9% for three junctions. *Nature Energy*, *2*(9), 17144. https://doi.org/10.1038/nenergy.2017.144

Fan, J., Jia, B., & Gu, M. (2014). Perovskite-based low-cost and high-efficiency hybrid

halide solar cells. *Photonics Research*, *2*(5), 111. https://doi.org/10.1364/PRJ.2.000111

Fru, J. (2016). *EFFECT OF ANNEALING TEMPERATURE ON THE FORMATION OF METHYL-AMMONIUM TIN TRI-IODIDE PEROVSKITE THIN FILM*.

Gail Overton. (2006). Quantum Dots promise - next-generation solar cells. *Photonics & Optoelectronics*, *42*(4). Retrieved from https://www3.nd.edu/~pkamat/pdf/laserfocus06.pdf

Graham Zabel. (2009). Peak People: The Interrelationship between Population Growth and Energy Resources - Resilience. Retrieved October 2, 2017, from http://www.resilience.org/stories/2009-04-20/peak-people-interrelationship-between-population-growth-and-energy-resources/

Green Energy. (2015). How Do Photovoltaic (PV) Solar Cells Work? Retrieved October 2, 2017, from http://cleangreenenergyzone.com/how-do-photovoltaic-pv-solar-cells-work/

Heo, J. H., Im, S. H., Noh, J. H., Mandal, T. N., Lim, C.-S., Chang, J. A., … Seok, S. Il. (2013). Efficient inorganic–organic hybrid heterojunction solar cells containing perovskite compound and polymeric hole conductors. *Nature Photonics*, *7*(6), 486–491. https://doi.org/10.1038/nphoton.2013.80

Holdren, J. P. (1991). Population and the energy problem. *Population and Environment*, *12*(3), 231–255. https://doi.org/10.1007/BF01357916

Hsiao, Y.-C., Wu, T., Li, M., Liu, Q., Qin, W., & Hu, B. (2015). Fundamental physics behind high-efficiency organo-metal halide perovskite solar cells. *Journal of Materials Chemistry A*, *3*(30), 15372–15385. https://doi.org/10.1039/C5TA01376C

Im, J.-H., Lee, C.-R., Lee, J.-W., Park, S.-W., & Park, N.-G. (2011). 6.5% efficient perovskite quantum-dot-sensitized solar cell. *Nanoscale*, *3*(10), 4088. https://doi.org/10.1039/c1nr10867k

International Energy Agency. (2016). World Energy Outlook 2016. Retrieved October 2, 2017, from https://www.iea.org/newsroom/news/2016/november/world-energy-outlook-2016.html

ISE, F. I. for S. E. S. (2017). Photovoltaics Rerport - 2017, (July), 44. Retrieved from https://www.ise.fraunhofer.de/content/dam/ise/de/documents/publications/studies/Photovoltaics-Report.pdf

ITACA. (2017). Part 2: Solar Energy Reaching The Earth's Surface | ITACA. Retrieved October 2, 2017, from http://www.itacanet.org/the-sun-as-a-source-of-energy/part-2-solar-energy-reaching the-earths-surface/

Jasim, K. E. (2015). Quantum Dots Solar Cells. In *Solar Cells - New Approaches and Reviews*. InTech. https://doi.org/10.5772/59159

Jeon, N. J., Noh, J. H., Kim, Y. C., Yang, W. S., Ryu, S., & Seok, S. Il. (2014). Solvent engineering for high-performance inorganic–organic hybrid perovskite solar cells. *Nature Materials*, *13*(9), 897–903. https://doi.org/10.1038/nmat4014

Jimoh, M. F. (2014). *Effects of Bending and Stretching on Hybrid Organic- Inorganic Trihalide Perovskite Solar Cells*. African University of Science and Technology, Abuja, Nigeria.

Kim, H.-B., Choi, H., Jeong, J., Kim, S., Walker, B., Song, S., & Kim, J. Y. (2014). Mixed solvents for the optimization of morphology in solution-processed, inverted-type perovskite/fullerene hybrid solar cells. *Nanoscale*, *6*(12), 6679. https://doi.org/10.1039/c4nr00130c

Kim, H.-S., Lee, C.-R., Im, J.-H., Lee, K.-B., Moehl, T., Marchioro, A., … Park, N.-G. (2012). Lead Iodide Perovskite Sensitized All-Solid-State Submicron Thin Film Mesoscopic Solar Cell with Efficiency Exceeding 9%. *Scientific Reports*, *2*(1), 591. https://doi.org/10.1038/srep00591

Kim, J. H., Liang, P.-W., Williams, S. T., Cho, N., Chueh, C.-C., Glaz, M. S., … Jen, A. K.-Y. (2015). High-Performance and Environmentally Stable Planar Heterojunction Perovskite Solar Cells Based on a Solution-Processed Copper-Doped Nickel Oxide Hole-Transporting Layer. *Advanced Materials*, *27*(4), 695–701. https://doi.org/10.1002/adma.201404189

Kojima, A., Teshima, K., Shirai, Y., & Miyasaka, T. (2009). Organometal halide perovskites as visible-light sensitizers for photovoltaic cells. *Journal of the American Chemical Society*, *131*(17), 6050–6051. https://doi.org/10.1021/ja809598r

Lee, C.-P., Li, C.-T., & Kuo-ChuanHo. (2017). Use of organic materials in dye-sensitized solar cells. *Materials Today*, *20*(5), 267–283. https://doi.org/10.1016/J.MATTOD.2017.01.012

Lee, M. M., Teuscher, J., Miyasaka, T., Murakami, T. N., & Snaith, H. J. (2012). Efficient Hybrid Solar Cells Based on Meso-Superstructured Organometal Halide Perovskites. *Science*, *338*(6107), 643–647. https://doi.org/10.1126/science.1228604

Li, Cong., Guo, Q., Wang, Z., Bai, Y., Liu, L., Wang, F.,Tan, Z. (2017). Efficient Planar Structured Perovskite Solar Cells with Enhanced Open-Circuit Voltage and Suppressed Charge Recombination Based on a Slow Grown Perovskite Layer from Lead Acetate Precursor. *ACS Applied Materials & Interfaces*, acsami.7b15229. https://doi.org/10.1021/acsami.7b15229

Li, Ming-Hsien., Shen, P., Wang, K., Guo, T., & Chen, P. (2015). Correction: Inorganic p-type contact materials for perovskite-based solar cells. *J. Mater. Chem. A*.

Li, Wenzhe., Fan, J., Li, J., Mai, Y., & Wang, L. (2015). Controllable grain morphology of perovskite absorber film by molecular self-assembly toward efficient solar cell exceeding 17%. *Journal of the American Chemical Society*, *137*(32), 10399–10405. http://doi.org/10.1021/jacs.5b06444

Li, Yi., Zhu, J., Huang, Y., Liu, F., Lv, M., Chen, S., … Dai, S. (2015). Mesoporous SnO_2 nanoparticle films as electron-transporting material in perovskite solar cells. *RSC Advances*, *5*(36), 28424–28429. http://doi.org/10.1039/C5RA01540E

Liu, J., Wu, Y., Qin, C., Yang, X., Yasuda, T., Islam, A., … Han, L. (2014). A dopant-free hole-transporting material for efficient and stable perovskite solar cells. *Energy Environ. Sci.*, *7*(9), 2963–2967. https://doi.org/10.1039/C4EE01589D

Liu, M., Johnston, M. B., & Snaith, H. J. (2013). Efficient planar heterojunction perovskite solar cells by vapour deposition. *Nature*, *501*(7467), 395–398. https://doi.org/10.1038/nature12509

Liu, Y., Sun, J., Yang, Z., Yang, D., Ren, X., Xu, H., … Liu, S. F. (2016). 20-mm-Large Single-Crystalline Formamidinium-Perovskite Wafer for Mass Production of Integrated Photodetectors. *Advanced Optical Materials*, *4*(11), 1829–1837. https://doi.org/10.1002/adom.201600327

Liu, Z. (2015). *Global energy interconnection*.

Mahmood, K., Sarwar, S., & Mehran, M. T. (2017). Current status of electron transport layers in perovskite solar cells: materials and properties. *RSC Adv.*, *7*(28), 17044–

17062. https://doi.org/10.1039/C7RA00002B

Marcin Majka, & Tomasz M. Majka. (2013). Healthy light source. Retrieved October 2, 2017,from https://www.researchgate.net/publication/255989402_Healthy_light_source

Meillaud, F., Boccard, M., G.Bugnon, Despeisse, M., & Al., S. H. et. (2015). Recent advances and remaining challenges in thin-film silicon photovoltaic technology. *Materials Today*, *18*(7), 378–384. https://doi.org/10.1016/J.MATTOD.2015.03.002

Mitch Jacoby. (2016). The future of low-cost solar cells. *American Chemical Society*, *94*(18), 30–35.

Mohammad Tawheed Kibria, Akil Ahammed, Mahmud Saad, & Shams-Ul-Islam Hossain. (2015). A Review: Comparative studies on different generation solar cells technology. In *5th International Conference on Environmental Aspects of Bangladesh [ICEAB]* . Retrieved from https://www.researchgate.net/publication/274195294_A_Review_Comparative_studies_on_different_generation_solar_cells_technology

National Geographic Society. (2017). air mass -. Retrieved October 2, 2017, from https://www.nationalgeographic.org/encyclopedia/air-mass/

National Instruments. (2017). Part II – Photovoltaic Cell I-V Characterization Theory and LabVIEW Analysis Code - National Instruments. Retrieved November 9, 2017, from http://www.ni.com/white-paper/7230/en/#top

National Renewable Energy Laboratory. (2017). Hybrid Tandem Solar Cells | Photovoltaic Research | NREL. Retrieved October 6, 2017, from https://www.nrel.gov/pv/hybrid-tandem-solar-cells.html

Nozik, A. J. (2002). Quantum dot solar cells. *Physica E: Low-Dimensional Systems and Nanostructures*, *14*(1–2), 115–120. https://doi.org/10.1016/S1386-9477(02)00374-0

NREL. (2017). Solar Energy Basics. Retrieved October 2, 2017, from https://www.nrel.gov/workingwithus/re-solar.html

Oku, T., Matsumoto, T., Suzuki, A., & Suzuki, K. (2015). Fabrication and Characterization of a Perovskite-Type Solar Cell with a Substrate Size of 70 mm. *Coatings*, *5*(4), 646–655. https://doi.org/10.3390/coatings5040646

Qin, P., Tanaka, S., Ito, S., Tetreault, N., & Manabe, K. (2014). Inorganic hole

conductor-based lead halide perovskite solar cells with 12.4% conversion efficiency. *Nature*.

Rand, B., & Richter, H. (2014). *Organic Solar Cells: fundamentals, devices, and upscaling*.

Ruy S. Bonilla, Reichel, C., Hermle, M., & Wilshaw, P. R. (2012). *Surface Passivation for Silicon Solar Cells*. Retrieved from http://semiconductor.materials.ox.ac.uk/research/current/surface-passivation.html

Saliba, M., Matsui, T., Seo, J.-Y., Domanski, K., Correa-Baena, J.-P., Nazeeruddin, M. K., … Grätzel, M. (2016). Cesium-containing triple cation perovskite solar cells: improved stability, reproducibility and high efficiency. *Energy & Environmental Science*, *9*(6), 1989–1997. https://doi.org/10.1039/c5ee03874j

Savva, A., Burgués-Ceballos, I., & Choulis, S. A. (2016). Improved Performance and Reliability of *p-i-n* Perovskite Solar Cells via Doped Metal Oxides. *Advanced Energy Materials*, *6*(18), 1600285. https://doi.org/10.1002/aenm.201600285

Singh, T. B., Marjanovi, N., Matt, G. J., Gü Nes, S., Sariciftci, N. S., Ramil, A. M., … Bauer, S. (2005). High-mobility n-channel organic field-effect transistors based on epitaxially grown C 60 films. https://doi.org/10.1016/j.orgel.2005.03.006

Song, T.-B., Chen, Q., Zhou, H., Jiang, C., Wang, H.-H., (Michael) Yang, Y., … Yang, Y. (2015). Perovskite solar cells: film formation and properties. *Journal of Materials Chemistry A*, *3*(17), 9032–9050. https://doi.org/10.1039/C4TA05246C

Song, Z., Watthage, S. C., Phillips, A. B., & Heben, M. J. (2016). Pathways toward high-performance perovskite solar cells: review of recent advances in organo-metal halide perovskites for photovoltaic applications. *Journal of Photonics for Energy*, *6*(2), 022001. https://doi.org/10.1117/1.JPE.6.022001

Sten Odenwald's. (2017). How much Energy does the sun produce in one hour. Retrieved October 2, 2017, from http://www.astronomycafe.net/FAQs/q1835x.html

Sum, T. C., & Mathews, N. (2014). Advancements in perovskite solar cells: photophysics behind the photovoltaics. *Energy Environ. Sci.*, *7*(8), 2518–2534. https://doi.org/10.1039/C4EE00673A

Tang, H., He, S., & Peng, C. (2017). A Short Progress Report on High-Efficiency Perovskite Solar Cells. *Nanoscale Research Letters*, *12*(1), 410.

https://doi.org/10.1186/s11671-017-2187-5

Vatansever, D., Siores, E., & Shah, T. (2012). Alternative Resources for Renewable Energy: Piezoelectric and Photovoltaic Smart Structures. In *Global Warming--Impacts and Future Perspective* (pp. 1–29). INTECH. https://doi.org/10.5772/50570

Wadia, C., Alivisatos, A. P., & Kammen, D. M. (2009). Materials availability expands the opportunity for large-scale photovoltaics deployment. *Environmental Science & Technology*, *43*(6), 2072–2077. Retrieved from http://www.ncbi.nlm.nih.gov/pubmed/19368216

Wang, D., Wright, M., Elumalai, N. K., & Uddin, A. (2016). Stability of perovskite solar cells. *Solar Energy Materials and Solar Cells*, *147*, 255–275. https://doi.org/10.1016/j.solmat.2015.12.025

Watthage, S. C., Song, Z., Liyanage, G. K., Phillips, A. B., & Heben, M. J. (2016). Investigation on the nucleation and growth mechanisms of perovskite formation in the two-step solution process. *Conference Record of the IEEE Photovoltaic Specialists Conference*, *2016–Novem*, 831–834. https://doi.org/10.1109/PVSC.2016.7749723

Wei, D. (2010). Dye sensitized solar cells. *International Journal of Molecular Sciences*, *11*(3), 1103–1113. https://doi.org/10.3390/ijms11031103

Will Soutter. (2013). What is a Dye-Sensitized Solar Cell? Retrieved October 5, 2017, from https://www.azonano.com/article.aspx?ArticleID=3175

Wojciechowski, K., Saliba, M., & Leijtens, T. (2014). Sub-150 C processed meso-superstructured perovskite solar cells with enhanced efficiency. *& Environmental ….*

World-nuclear association. (2017). World Energy Needs and Nuclear Power | Energy Needs | Nuclear Energy meeting Energy Needs - World Nuclear Association. Retrieved October 2, 2017, from http://www.world-nuclear.org/information-library/current-and-future-generation/world-energy-needs-and-nuclear-power.aspx

Worldometers. (2017). World Population Clock: 7.6 Billion People (2017) - Worldometers. Retrieved October 2, 2017, from http://www.worldometers.info/world-population/

Xiao, Z., Yuan, Y., Wang, Q., Shao, Y., Bai, Y., Deng, Y., … Huang, J. (2016). Thin-film

semiconductor perspective of organometal trihalide perovskite materials for high-efficiency solar cells. *Materials Science and Engineering R: Reports*, *101*, 1–38. https://doi.org/10.1016/j.mser.2015.12.002

Xu, M., Feng, J., Ou, X. L., Zhang, Z. Y., Zhang, Y. F., Wang, H. Y., & Sun, H. B. (2016). Surface Passivation of Perovskite Film by Small Molecule Infiltration for Improved Efficiency of Perovskite Solar Cells. *IEEE Photonics Journal*, *8*(5). https://doi.org/10.1109/JPHOT.2016.2608619

Yan, J., & Saunders, B. R. (2014). Third-generation solar cells: a review and comparison of polymer:fullerene, hybrid polymer and perovskite solar cells. *RSC Adv.*, *4*(82), 43286–43314. https://doi.org/10.1039/C4RA07064J

Yang, G., Tao, H., Qin, P., Ke, W., & Fang, G. (2016). Recent progress in electron transport layers for efficient perovskite solar cells. *Journal of Materials Chemistry A*, *4*(11), 3970–3990. https://doi.org/10.1039/C5TA09011C

Yang, L., Barrows, A. T., Lidzey, D. G., & Wang, T. (2016). Recent progress and challenges of organometal halide perovskite solar cells. *Reports on Progress in Physics*, *79*(2), 026501. https://doi.org/10.1088/0034-4885/79/2/026501

Yang, W. S., Noh, J. H., Jeon, N. J., Kim, Y. C., Ryu, S., Seo, J., & Seok, S. I. (2015). High-performance photovoltaic perovskite layers fabricated through intramolecular exchange. *Science*, *348*(6240), 1234–1237. https://doi.org/10.1126/science.aaa9272

Yang, W. S., Park, B.-W., Jung, E. H., Jeon, N. J., Kim, Y. C., Lee, D. U., … Seok, S. Il. (2017). Iodide management in formamidinium-lead-halide–based perovskite layers for efficient solar cells. *Science*, *356*(6345), 1376–1379. https://doi.org/10.1126/science.aan2301

Yifan Li. (2016). High Performance Perovskite Hybrid Solar Cell Via Interfacial Engineering

Yahui Li., Zhao, Z., Lin, F., Cao, X., Cui, X., & Wei, J. (2017). In Situ Observation of Crystallization of Methylammonium Lead Iodide Perovskite from Microdroplets, 1–7. https://doi.org/10.1002/smll.201604125

Zeng, W., Liu, X., Guo, X., Niu, Q., Yi, J., Xia, R., … Kim, H. (2017). Morphology analysis and optimization: Crucial factor determining the performance of perovskite

solar cells. *Molecules*, *22*(4), 1–23. https://doi.org/10.3390/molecules22040520

Zhang, W., Saliba, M., Moore, D. T., Pathak, S. K., Hörantner, M. T., Stergiopoulos, T., … Snaith, H. J. (2015). Ultrasmooth organic–inorganic perovskite thin-film formation and crystallization for efficient planar heterojunction solar cells. *Nature Communications*, *6*, 6142. https://doi.org/10.1038/ncomms7142

Zhao, L., Luo, D., Wu, J., Hu, Q., Zhang, W., Chen, K., … Gong, Q. (2016). High-Performance Inverted Planar Heterojunction Perovskite Solar Cells Based on Lead Acetate Precursor with Efficiency Exceeding 18%. *Advanced Functional Materials*, *26*(20), 3508–3514. https://doi.org/10.1002/adfm.201601175

Zheng, L., Zhang, D., Ma, Y., Lu, Z., Chen, Z., Wang, S., … Gong, Q. (2015). Morphology control of the perovskite films for efficient solar cells. *Dalton Trans.*, *44*(23), 10582–10593. https://doi.org/10.1039/C4DT03869J

Zheng, Z., Ji, H., Yu, P., & Wang, Z. (2016). Recent Progress Towards Quantum Dot Solar Cells with Enhanced Optical Absorption. *Nanoscale Research Letters*, *11*(1), 266. https://doi.org/10.1186/s11671-016-1457-y

Zhou, H., Chen, Q., Li, G., Luo, S., Song, T. -b., Duan, H.-S., … Yang, Y. (2014). Interface engineering of highly efficient perovskite solar cells. *Science*, *345*(6196), 542–546. https://doi.org/10.1126/science.1254050

Zulkifli, M. H., & Bahtiar, A. (2016). Optical and structural properties of perovskite films prepared with two-step spin-coating method, *050012*, 050012. https://doi.org/10.1063/1.4941895

Zuo, L., Dong, S., De Marco, N., Hsieh, Y. T., Bae, S. H., Sun, P., & Yang, Y. (2016). Morphology Evolution of High Efficiency Perovskite Solar Cells via Vapor Induced Intermediate Phases. *Journal of the American Chemical Society*, *138*(48), 15710–15716. https://doi.org/10.1021/jacs.6b09656